EUTECTIC SUPERALLOYS BY EDGE-DEFINED, FILM-FED GROWTH

G. F. Hurley
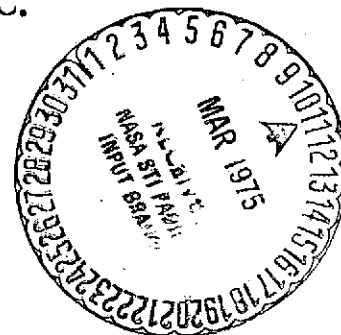
January 1975

TYCO LABORATORIES, INC.

Prepared for

NASA-Lewis Research Center

Contract NAS 3-16790

1. Report No. NASA CR-134756	2. Government Accession No.	3. Recipient's Catalog No.
4. Title and Subtitle Eutectic Superalloys by Edge-Defined, Film-Fed Growth		5. Report Date January 1975
		6. Performing Organization Code
7. Author(s) G. F. Hurley		8. Performing Organization Report No. C-325
9. Performing Organization Name and Address Tyco Laboratories, Inc. 16 Hickory Drive Waltham, Massachusetts 02154		10. Work Unit No.
		11. Contract or Grant No. NAS3-16790
12. Sponsoring Agency Name and Address National Aeronautics and Space Agency Washington, D. C. 20546		13. Type of Report and Period Covered Contractor Report
		14. Sponsoring Agency Code

15. Supplementary Notes

Project Manager, Fredric H. Harf, Materials and Structures Division
NASA Lewis Research Center, Cleveland, Ohio

16. Abstract   A program with the objective of establishing the feasibility of producing directionally soli-
dified eutectic alloy composites by edge-defined, film-fed growth (EFG) was carried out. In the first
half of the program research to identify and characterize die materials was conducted. In the second
part of the program, three eutectic alloys were grown using one of the die materials identified.

The three eutectic alloys which were investigated were $\gamma + \delta$, $\gamma/\gamma' + \delta$, and a Co-base TaC
alloy containing Cr and Ni. Investigations into the compatibility and wettability of these metals with
various carbides, borides, nitrides, and oxides disclosed that compounds with the largest (negative)
heats of formation were most stable but poorest wetting. Nitrides and carbides had suitable stability
and low contact angles but capillary rise was observed only with carbides. Oxides would not give
capillary rise but would probably fulfil the other wetting requirements of EFG. Tantalum carbide was
selected for most of the experimental portion of the program based on its exhibiting spontaneous
capillary rise and satisfactory slow rate of degradation in the liquid metals.

Samples of all three alloys were grown by EFG with the major experimental effort restricted
to $\gamma + \delta$ and $\gamma/\gamma' + \delta$ alloys. In the standard, uncooled EFG apparatus, the thermal gradient was
inferred from the growth speed and was 150 to 200°C/cm. This value may be compared to typical
gradients of less than 100°C/cm normally achieved in a standard Bridgman-type apparatus. When a
stream of helium was directed against the side of the bar during growth, the gradient was found to
improve to about 250°C/cm. In comparison, a theoretical gradient of 700°C/cm should be possible
under ideal conditions, without the use of chills. Methods for optimizing the gradient in EFG are dis-
cussed, and should allow attainment of close to the theoretical for a particular configuration.

17. Key Words (Suggested by Author(s)) Edge-defined, film-fed growth Composites Cobalt Alloys Eutectics Refractory Compounds Solidification Tantalum Carbide Nickel Alloys	18. Distribution Statement Unclassified-Unlimited

19. Security Classif. (of this report) UNCLASSIFIED	20. Security Classif. (of this page) UNCLASSIFIED	21. No. of Pages 83	22. Price* Domestic $3.75 Foreign $6.25

NASA-C-168 (Rev. 6-71)

Table of Contents

List of Illustrations

List of Illustrations (continued)

List of Tables

SUMMARY

A two-part program was carried out to establish the feasibility of producing directionally solidified eutectic alloy composites by the edge-defined, film-fed growth process (EFG). In the EFG process, the liquid alloy is conducted to the top surface of a die by capillarity and growth occurs from a film of liquid (meniscus) on top of the die. The determination of a die material wetted by and chemically inert to the liquid alloy formed the first major task of the program. Since most eutectic alloys of interest require steep temperature gradients for plane front solidification, the second major task of the program was to show that suitable temperature gradients could be attained.

The three eutectic alloys which were investigated were $\gamma + \delta$, $\gamma/\gamma' + \delta$, and a Co-base TaC alloy containing Cr and Ni. Investigations into the compatibility and wettability of these metals with various carbides, borides, nitrides, and oxides were carried out by means of soaking tests in which sample coupons were held in contact with the molten alloys for periods up to 5 hr. Metallographic examination was subsequently used to determine the nature and extent of the interaction. These investigations disclosed that compounds with the largest (negative) heats of formation were most stable but poorest wetting. Nitrides and carbides had suitable stability and low contact angles but capillary rise was observed only with carbides. Oxides would not give capillary rise but would probably fulfil the other wetting requirements of EFG. Tantalum carbide was selected for most of the experimental portion of the program based on its exhibiting spontaneous capillary rise and satisfactory slow rate of degradation in the liquid metals.

HfC behaved similarly to TaC but quickly plugged up during growth runs. The only other material successfully used in growth trials was tungsten. In this case lifetime of the die was limited to one to two hours by its rate of dissolution in the melt.

Samples of all three alloys were grown by EFG with the major experimental effort restricted to $\gamma + \delta$ and $\gamma/\gamma' + \delta$ alloys. In the standard, uncooled EFG apparatus, the thermal gradient was inferred from the growth speed and was 150 to 200°C/cm. This value may be compared to typical gradients of less than 100°C/cm normally achieved in a standard Bridgman-type apparatus. When a stream of helium was directed against the side of the bar during growth, the gradient was found to improve to about 250°C/cm. In comparison, a theoretical gradient of 700°C/cm should be possible under ideal conditions, without the use of chills.

Methods for optimizing the gradient in EFG are discussed and would include both modifications to the set-up and fuller exploitations to a cooling system. Thermal gradient measurements above EFG set-ups at slightly higher temperatures, have shown attainment of 600°C/cm at zero growth rate.

I. INTRODUCTION

Research into high temperature materials for gas turbine engines has resulted in a steady improvement in properties, and consequently, in increased operating temperatures. In the course of this development activity, compositional changes have accounted for some of the improvements. Directional solidification has been a key processing change which has resulted in improved properties through control of the microstructure, in conventional superalloys.

Composite materials have been considered as alternatives to ordinary alloy development, especially as the upper bounds for super alloy performance were approached. Here a fibrous form of a strong and heat resistant material would be used to reinforce an oxidation resistant matrix material. However, although several low temperature composite systems have been developed, there has as yet been no outstanding success toward achieving high temperature composite materials suitable for turbine hardware. One of the difficulties in this approach has been the expensive nature of the hybrid composite systems which have been considered. A second difficulty has been choice of a fiber-matrix system in which the constituents were mutually chemically compatible.

The formation of in situ composites by the directional solidification of eutectic alloys has offered an approach toward optimization of system compatibility. Work on a large number of eutectic systems has shown that while no simple systems are available with potential for producing satisfactory properties, alloying additions can be made which improve system properties. Further, these alloyed systems can be solidified in steep thermal gradients, to yield composite structures potentially capable of high performance in engine environments. Research in recent years has therefore followed the approach of investigating the effects of alloying changes on properties in particular systems.

3

While no one material is yet available which combines all necessary properties to qualify for gas turbine application (ref. 1), two systems in particular are considered to merit attention. One such system is the lamellar eutectic based on additions of Cr and Al to Ni-Ni$_3$Cb ($\gamma + \delta$). An advanced variation of this system is the $\gamma/\gamma' + \delta$ alloy which contains γ' precipitates to strengthen the γ-phase lamellae. A second system which is considered to possess some merit is based on TaC with a Ni or Co based matrix. This fibrous eutectic alloy is not so far advanced toward engine application as $\gamma/\gamma' + \delta$, but is nevertheless of exceptional interest.

Processing of directionally solidified alloys has been primarily by the Bridgman method (ref. 2). This area is one in which problems exist in some cases and in which flexibility and improvements could follow from the advances in processing techniques. Thus, for example, mold-metal interactions which produce a skin effect in some alloys, the ability to produce shapes, and the ability to produce steep thermal gradients are examples of problems or limitations of conventional processing which might be expected to be improved by processing changes.

This report describes an initial investigation of the feasibility of applying a new method of processing, edge-defined, film-fed growth (EFG), to the growth of eutectic alloys chosen from two classes of alloys named above. The basis characteristics of and requirements for, EFG are given in Appendix A. Our objectives were to show that die materials essential for EFG processing, could be found, and that directionally solidified bars could be produced using materials identified in this investigation.

EFG processing has potential for directional solidification of eutectic alloys for the following reasons:

● The absence of a crucible in the region undergoing solidification removes an important impediment to heat removal and should allow a concomitant gain in thermal gradient and thus, growth rate.

● The capability of growing shaped bodies directly could lead to cost savings by not requiring a new mold and core for each piece grown.

● The capability of growing hollow shapes directly could result in more attractive growth rates since heat can be extracted from the center as well as the edges of the shape.

4

● The configuration of the heat flow is likely to produce axial heat flow and thus a superior structure.

The emphasis in this study has been to investigate candidate die materials in order to find one or more materials best suited for growth of the $\gamma/\gamma' + \delta$ and Co-TaC alloys considered. Criteria here were chemical compatibility and wettability. In the second half of the investigation, growth trials emphasizing the effect of setup variables on structure were carried out.

II. EXPERIMENTAL PROCEDURE

2.1 Alloy Selection and Preparation

Three alloys were considered in this investigation and are listed in Table I. These alloys represent two major classes of lamellar and fibrous eutectic alloys which are considered to have potential merit. The first alloy was used in most of the initial growth trials while the $\gamma/\gamma' + \delta$ and Co-TaC alloys were studied in the optimization phase of the growth trials.

Table I. Alloy Compositions

Weight percent

Alloy	Ni	Cr	Co	Cb	Al	Ta	C
$\gamma + \delta$	76.5	-	-	23.5	-	-	-
$\gamma/\gamma' + \delta$	71.8	6	-	19.7	2.5	-	-
Co-TaC	25	15	47.2	-	-	12	0.8

Master melts of the three alloys were prepared by melting, in high purity alumina crucibles, the charge elements with purities noted in Table II. Appropriate quantities of each element or compound were placed in the crucible within the vacuum induction melting apparatus. The system was evacuated, flushed, and back-filled with Ar. Each alloy was heated until observed to be molten, then held at approximately 100°C above the liquidus for 15 minutes before turning off the power. Alloys for the compatibility trials were cooled in the crucible. Alloys used for growth trials were poured into a chilled quartz crucible. Ingots prepared in this way were then surface ground and sliced into sizes appropriate for compatibility or growth experiments.

2.2 Compatibility and Wetting Trials

Various carbides, borides, nitrides, oxides, and elemental materials were selected for evaluation as candidate die materials. These materials were obtained as hot pressed discs with average dimensions of 5.1 cm diameter and 0.65 cm thickness, and had densities of approximately 82 to 96% of theoretical. Oxides and elemental materials (W and C) were obtained as high purity, fully consolidated bodies. Both coarse grained and fine grained (Poco) graphites were used.

At the beginning of the program, all of the materials available or under consideration at that time were screened by means of 1 hr soak trials. In these tests, samples were excised from the starting billets and placed on a flat alumina plate. A small chip of metal was placed on the test coupon and the whole assembly was heated in the apparatus shown in Fig. 1. In this setup a molybdenum susceptor containing the sample was placed within a water-cooled, double wall quartz muffle. The susceptor was heated by rf inductance from a coil external to the chamber. The work was viewed by means of a window port in the chamber facing a slot cut in the susceptor wall, and temperature was monitored by means of a thermocouple inserted against the bottom of the alumina plate. through the bottom of the susceptor. The work was protected from oxidation by means of an Ar-5% H_2 gas stream flowing through the chamber. Power was increased to bring the temperature to approximately 100°C above the liquidus temperature of the alloy, and was held for 1 hr.

After these initial screening trials, a second series of 5 hour soak tests was conducted on selected materials, further to evaluate their compatibility. The 5-hr soak tests were conducted in an apparatus similar to that used in the 1-hr compatibility trials. The most significant difference was modification of the molybdenum plug which

8

Table II. Purity of Charge Elements

	TaC[1]	Chromium[2] Flakes	Columbium[3]	Nickel[4]	Cobalt[5]	Aluminum[6]
Ag	-	-	-	2	-	-
Al	-	-	28	< 1	-	-
B	-	-	< 1	-	-	-
C	500 (free)	-	< 30	-	-	-
Ca	100	-	30	< 1	0.1	2
Cb	6000	-	Bal	-		
Cd	-	-	< 5	-	-	-
Co	-	-	< 10	-	Bal	-
Cr	-	-	< 20	-	-	-
Cu	-	-	< 40	1	0.1	3
Fe	600	10	< 50	10	5	4
Hf	-	-	< 50	-	-	-
H	-	1	< 5	-	-	-
K + Na	100	-	-	-	-	-
Mg	-	-	< 20	< 1	0.1	0.2
Mn	-	-	< 20	-	-	-
Mo	-	-	< 20	-	-	-
N	-	40	29	-	-	-
Ni	-	-	< 20	Bal	1	0.3
O	-	62	110	-	-	-
Pb	-	-	< 20	-	-	-
Si	200	10	< 50	< 1	8	4
Sn	-	-	< 10	-	-	-
Ta	-	-	900	-	-	-
Ti	500	-	< 40	-	-	-
V	-	-	< 20	-	-	-
W	-	-	140	-	-	-
Zr	-	-	< 100	-	-	-
Zn	-	-	-	-	-	3

[1] Alpha Inorganics

[2] Shield Alloy Corp.

[3] Teledyne, Wah Chang Co.

[4] United Mineral and Chemical Corp.

[5] United Mineral and Chemical Corp.

[6] United Mineral and Chemical Corp.
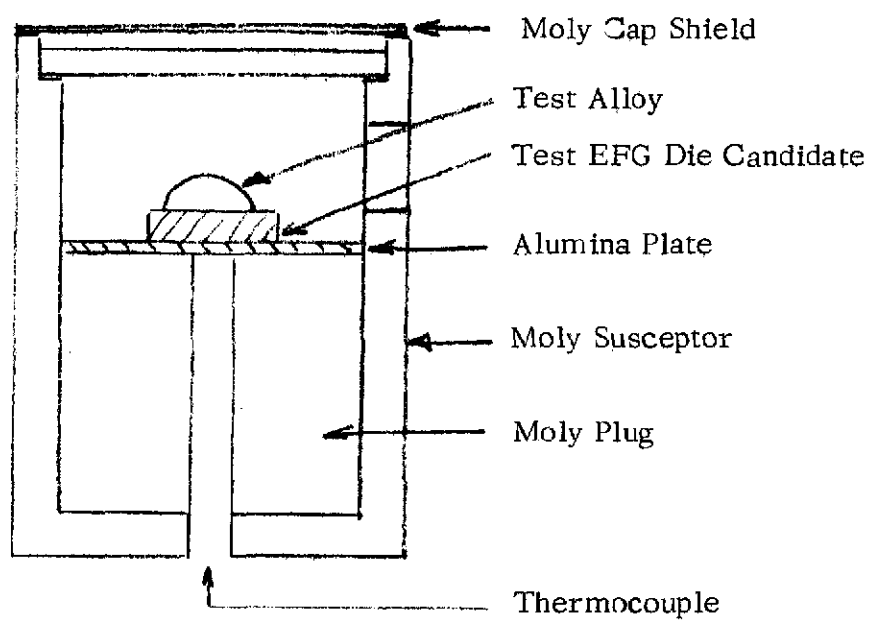
Fig. 1. Wetting test setup

fits within the susceptor to accept three 1-cm radius crucibles in drilled recesses. In this way, the sample, a metal-ceramic-metal sandwich, could be contained with good thermal contact to the heater, and more than one combination could be run simultaneously.

Tests were carried out as follows. A ceramic chip was sandwiched between two lumps of metal and placed in a small, stabilized zirconia crucible. In practice, one of the three alloys was chosen and combined with three different ceramics to fill the three stations in the setup. After suitable purging and evacuation of the furnace, the temperature was raised to 100°C greater than the alloy melting temperature and held for 5 hrs.

Upon the conclusion of either 1 hour or 5 hour compatibility trials, samples were evaluated by visual and by metallographic examination. Contact angles were measured and a qualitative measure of interaction was determined from the appearance of the microstructure.

2.3 Growth Apparatus and Trials

2.3.1 Pulling Frame

Growth experiments were conducted using a modified Czochralski puller with a 30 cm stroke, shown in Fig. 2. The work, including a pedestal to support the setup, the setup itself, and the seed, were contained within the quartz furnace enclosure described above. The pulling motion was accomplished by means of a pneumatic-hydraulic cylinder which allows a carriage to move upwards. Motion of this carriage was controllable for a speed range of less than 0.5 cm/hr to more than 300 cm/hr. Slow growth speeds were measured using a dial indicator and a stop watch. Faster growth speeds were measured similarly using a fixed tape measure.

The seed used to initiate growth was supported from the pulling carriage by means of a shaft which passed through a loose seal at the top of the furnace chamber.

The pedestal to support the setup is mounted on a carriage beneath the furnace enclosure. This fixture is lowered to install the setup and contains provision for gas inlet and a thermocouple.

2.3.2 Growth Setups

Growth was carried out using essentially standard EFG setups. These setups consisted of a molybdenum susceptor, an alumina crucible to contain the melt, a die-holding plate, and appropriate heat shielding. A thermocouple passing upwards

Fig. 2. Crystal growth apparatus

through the pedestal which supports the setup was inserted into an axial hole in the bottom of the susceptor and was used as a temperature reference.
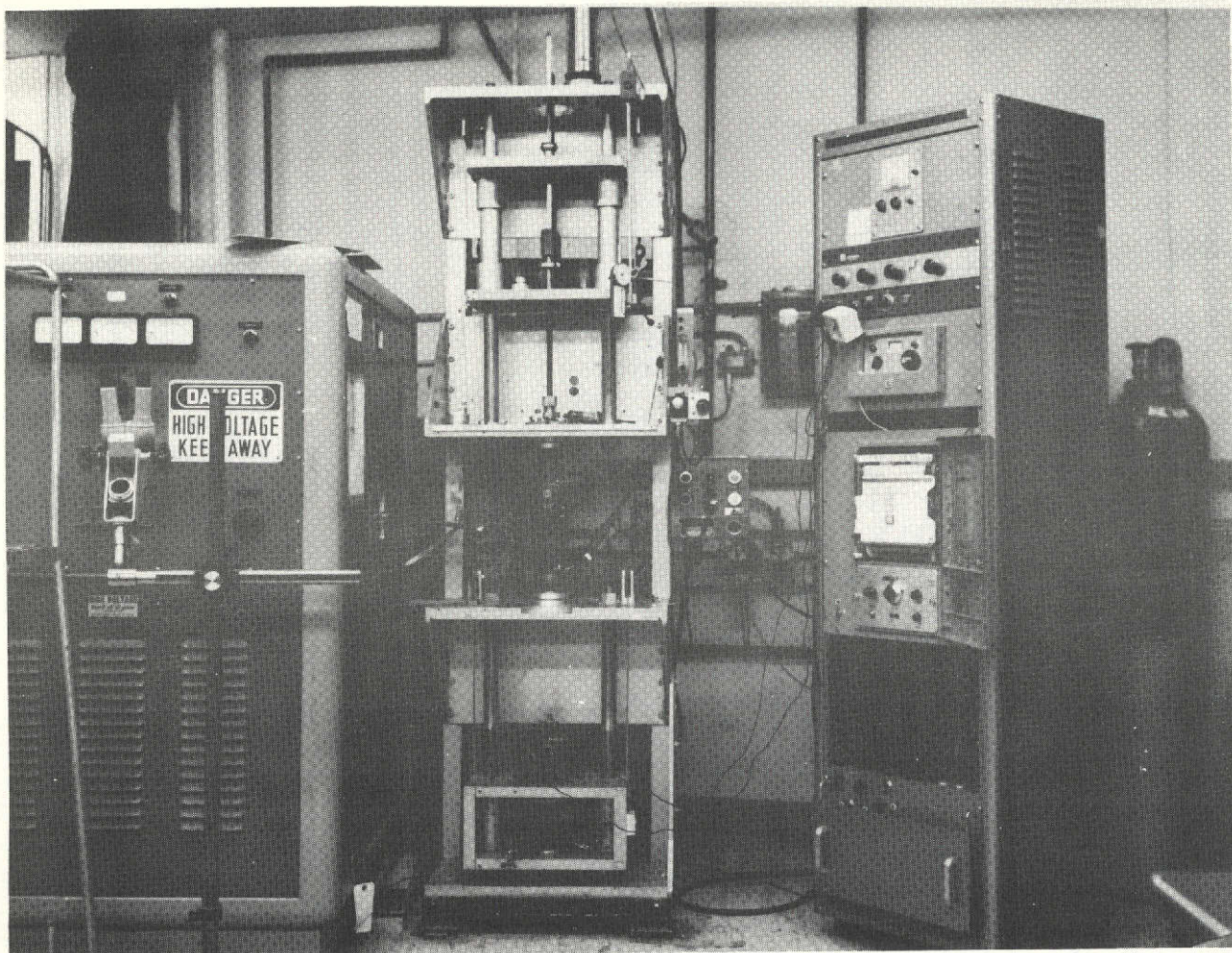
Two types of growth setups were used. Setups for rod growth where the die was tungsten or carbon, used a molybdenum die holding plate as illustrated in Fig. 3a. When the die was fabricated from TaC, however, a more elaborate holding plate was required due to metal seepage through the porous die. A typical ribbon-growing setup employing a TaC die and alumina spacers in the holding plate is shown in Fig. 3b.

Several different die types and designs were utilized and are described in Fig. 4. Rod-type orifices were prepared from carbon, tungsten, and TaC according to the designs shown in Fig. 4a, b, and c respectively. Fig. 4a was the design of choice but was found not to be fabricable by available technology from the materials of major interest (TaC, TiN). The design shown in Fig. 4c was not immediately successful due to feeding difficulties and uneven thermal distribution. One modification of this design was attempted in which three additional slots were cut at 90° intervals around the circumference.

Figs. 4d and e are the two ribbon-type dies which were fabricated and used. The design shown in Fig. 4d was found to be fragile and was replaced by the one shown in Fig. 4e. The latter was modified during the course of the program to provide for the growth of wider ribbons. This was particularly advantageous for the growth of $\gamma/\gamma' + \delta$. Dimensions of the various dies utilized are listed in Table III.

2.3.4 Growth Procedure

Prior to the start of each run, the crucible was charged with the pre-alloyed metal, and a seed was prepared, usually from a slice of the eutectic alloy. The crucible charge was prepared by cutting a disc of the alloy in half and grinding a cavity at the center for the bottom of the die. This allowed maximum volume of metal in the small setup employed. The seed was welded to a steel rod and was positioned on the end of the pull shaft. The system was flushed with a mixture of Ar-5% H_2. One exception to this procedure was used for experiments utilizing HfC dies. Here, pure Ar was used until after seeding, at which time the gas flow was switched to the standard mixture.

After flushing the system with the proper gas mixture, the temperature of the setup was raised by means of rf power from the external coil. In some cases of readily wetting dies, liquid is observed to appear at the top of the die feed slot when

Tungsten die   Heat shields

Holding Plate
Moly crucible

Al_2O_3 liner

Graphite susceptor

(a)
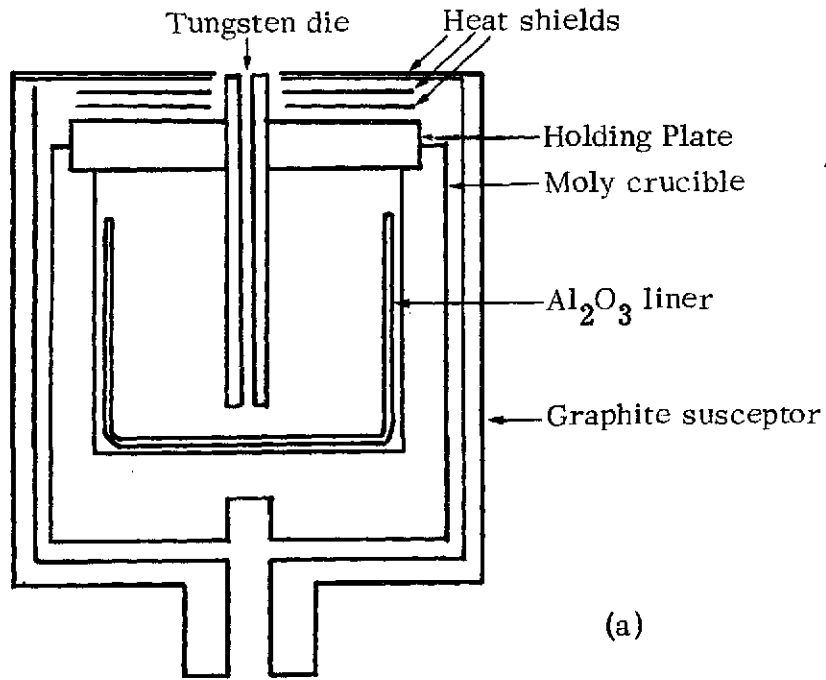
Rod growth setup utilizing all metal holding plate

Die Al_2O_3 Spacer

Heat Shield

Molybdenum Die Holding Plate

Al_2O_3 Crucible

Molybdenum Susceptor

Thermocouple Cavity

(b)
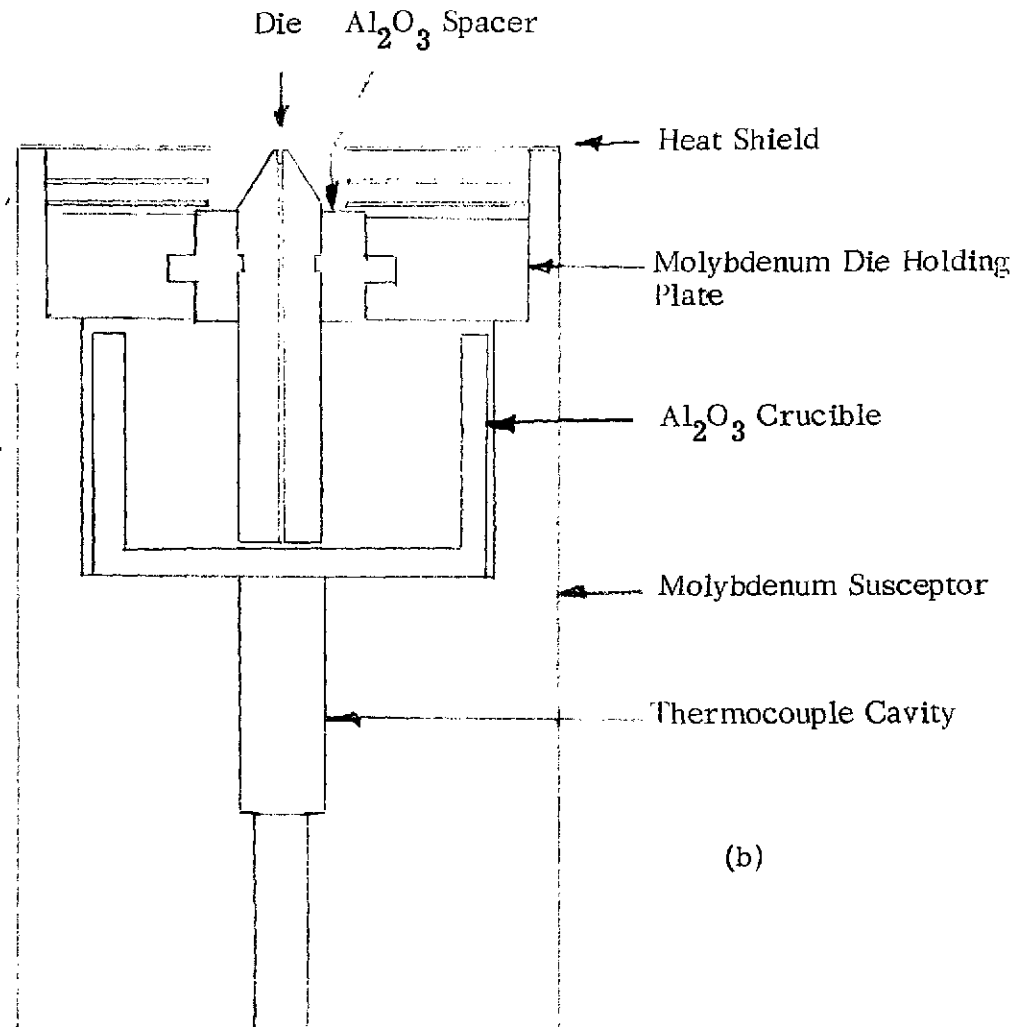
Ribbon growth setup utilizing alumina spacers in the holding plate

Fig. 3. Growth setups
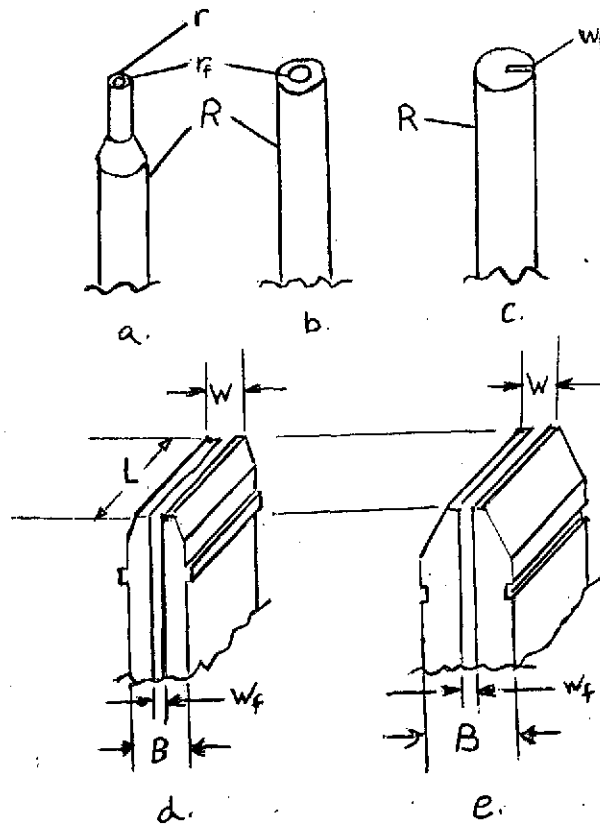
Fig. 4. Die configurations used (see Table III for dimensions)

Table III. Die Dimensions (cm)

Type*	Geometry	2R	r	r_f	W_f	W	L	B
a	Rod	0.32	0.12	0.051				
b	Rod	0.32	-	0.16				
c	Rod	$\begin{cases} 0.32 \\ 0.48 \\ 0.64 \end{cases}$	-	-	0.051 0.025			
d	Ribbon				0.025 0.037	0.05 0.19	0.58 0.58	0.19 0.19
e	Ribbon				0.025 0.05	0.05 0.15	0.58 0.58	0.4 0.4

*See Fig. 4.

15

the proper temperature was reached. In the general case, however, the liquid appeared more gradually and the proper temperature was reached by noting when seed melting on top of the die occurred, after the thermocouple reading had shown the crucible to have reached the melting temperature.

Seeding was accomplished by dipping the seed into the liquid at the top of the feed slot or by melting some of the seed to connect it with the liquid. Temperature was then adjusted as the seed was withdrawn to achieve shape control.

III. RESULTS AND DISCUSSION

3.1 Die Material Evaluation

3.1.1 Compatibility Investigations

The approach to the selection of die materials was to choose samples of the most refractory metals and compounds from those having the greatest thermodynamic stability. Tables IV to VII list all of the compound materials which were considered, and indicate those which were investigated as well as those for which previous data are available. Table VIII presents the initial evaluation of these materials, based on the 1 hr tests. These observations suggested that further work should be confined to the nitrides and carbides since oxides were not sufficiently wetted, and borides appeared reactive. The oxide materials were, however, judged fully compatible.

On the basis of these qualitative comparisons four materials, listed in Table IX, were selected for further evaluation including more extended compatibility trials and orifice fabrication. The more extended compatibility trials comprised 5-hr soak tests in which the candidate material was immersed in the liquid metal for 5-hr. In addition, the 1-hr compatibility trial samples were re-examined in order to measure the contact angle of the liquid metal on the ceramic.

After completion of the 5-hr soak, the samples were metallographically sectioned and examined microscopically. Each sample was classified according to four microstructural characteristics with results listed in Table IX. The extent of metal penetration into the ceramic was judged nearly complete, extensive, or slight, in the several cases. The extent of penetration is partly a function of the amount and nature of porosity in the ceramic, the wettability, and also may indicate the likelihood of grain boundary penetration. Surface integrity is a judgment of the degree to which the original surface had withstood erosion or dissolution in the liquid metal.

Table IV. Data on Refractory Oxides

Oxide	ΔH_f Kcal/mole	$T_{m.p.}$ °C
MgO	144	2650
Al_2O_3 *	400	2050
TiO_2 *	226	1870
ZrO_2	260	2720
HfO_2	266	2900
Cr_2O_3 ‡	270	(2400)

Table V. Data on Refractory Carbides

Carbide	ΔH_f Kcal/g-atom	Approximate m.p. °C
B_4C ‡	14	2450
SiC ‡	15	> 2700
TiC *	57	3140
ZrC*	48	3550
HfC *	81	3890
NbC*	33	3480
TaC*	38	3880
WC ‡	8.4	~2700

*These entries were selected for evaluation.
‡Data for these materials relative to similar alloys available from previous investigation.

Table VL Data on Refractory Nitrides

Nitride	$-\Delta H_f$ Kcal/g-atom	Approximate m.p. °C
BN*	60	-
TiN*	80.4	2950
ZrN	87.3	2980
HfN	88.2	3310
NbN	59	2050
TaN*	59	3090
WN	17	-

Table VIL Data on Refractory Borides

Borides	$-\Delta H_f$ Kcal/g-atom	Approximate m.p. °C
TiB$_2$*	24	2980
ZrB$_2$‡	26	3040
HfB$_2$*	-	3250
NbB$_2$	12	> 2900
TaB$_2$	17.5	3200
WB	-	2920

Table VIII. Summary of 1 hr Compatibility Trial Data
(atmosphere Ar + 5% H_2)

Die and Material	$\gamma + \delta$		$\gamma/\gamma' + \delta$		Co-TaC	
	Wetting	Gross Reaction	Wetting	Gross Reaction	Wetting	Gross Reaction
Al_2O_3	No	No	No	No	No	No
ZrO_2	No	No	No	No	No	No
TiB_2	Yes	Yes	Yes	Yes	Yes	Not observed
HfB_2	-	Yes	-	Yes	-	Yes
TaN	Yes	No	Yes	Some	Yes	?
BN	Yes	No	Yes	No	-	Yes
TiN	Yes	No	Yes	No	Yes	No
TaC	Yes	No	Yes	No	Yes	No
CbC	Yes	No	Yes	No	Yes	No
TiC	Yes	?	Yes	No	Yes	No
ZrC	Yes	?	Yes	No	Yes	No
HfC	Yes	No	Yes*	No	Yes	No

*Wetting was observed for Ar atmosphere only.

Table IX. Results of 5-hr Soak Tests (atmosphere Ar + 5% H_2)

Alloy Ceramic		No. 1 Ni-Cb	No. 2 Ni-Cb-Cr-Al	No. 3 Co-TaC
1. TiN	a*	Extensive	Nearly complete	Extensive
	b	Excellent	Poor	Fair
	c	Nil	Moderate	Nil
	d	Nil	Nil	Yes
2. TaC	a	Extensive	Slight	Slight
	b	Fair	Fair-to-good	Fair
	c	Slight	Nil	Slight
	d	Nil	Nil	Slight
3. CbC	a	Extensive	Slight	Nearly complete
	b	Good	Fair-to-good	Poor
	c	Nil	Slight	Moderate
	d	Nil	Nil	Large amounts
4. TiC	a	Carbide	†	
	b	Dispersed		
	c	Throughout		
	d	Metal		

*a   Extent of metal penetration into ceramic
 b   Surface integrity
 c   Grain separation
 d   Occurence of massive carbides or reprecipitated ceramic phase
†   Not attempted.

Grain separation refers to whether or not ceramic particles had separated from the ceramic and could be found in the metal. Finally, the fourth category notes whether or not the microstructure of the metal is altered in the vicinity of the ceramic.

Figs. 5 through 7 display varying behavior in these four categories. Fig. 5 shows extensive penetration of the metal into the ceramic, but it retained an excellent surface integrity, while no evidence of nitride separation or alteration of the microstructure was found. Fig. 6 showed only partial infiltration of the metal into the TaC ceramic, with fair retention of surface integrity and insignificant grain separation or microstructural changes. Fig. 7 is an example of an unacceptable combination in which the infiltration is nearly complete, the surface is poor, and both grain separation and massive carbide precipitation have occurred.

As a result of the 5-hr soak tests, only the combinations of the TaC containing alloy with CbC and the Ni-Cb alloy with TiC in Table IX were judged unacceptable among those previously thought to be possible combinations. TaC and TiN were judged a reasonable choice for any alloy, and CbC appeared feasible for all but the TaC-containing alloy.

One other refractory compound, in addition to TaC, TiN, and CbC, was considered acceptable on the basis of tests performed later in the program. HfC had not been available at the start of the experimental work and was subsequently investigated later in the program. The monocarbide alloy was found to interact with HfC during a 1 hr test and produced what appeared to be a mixed carbide layer on the surface of the alloy. Wetting was complete. Both $\gamma + \delta$ and $\gamma/\gamma' + \delta$ interacted little with HfC in one hour tests. Wetting was inconsistent but was found to improve in Ar compared to Ar + 5% H_2.

Additional 1 hr tests were carried out for the combinations graphite versus $\gamma + \delta$, and Co-TaC, and W versus $\gamma + \delta$. Fine grained graphite was found to react with $\gamma + \delta$ to form CbC with an effective contact angle of about 15°. One test with the Co-TaC alloy on a coarse grained graphite showed moderate erosion of the graphite. Tungsten exhibited intergranular penetration by liquid $\gamma + \delta$ but the surface retained its integrity. The wetting angle was close to zero. Table X summarizes the contact angle data for six materials of interest. Here TiN was found to have the highest contact angle, and TaC and W the lowest.

3.1.2 Preliminary Growth Trials

Growth trials were attempted using dies constructed of TiN, TaC, CbC, HfC, W, and C, primarily with the $\gamma - \delta$ alloy, in order to substantiate the

$\leftarrow \quad \gamma + \delta \quad$ eutectic

$\leftarrow \quad$ TiN
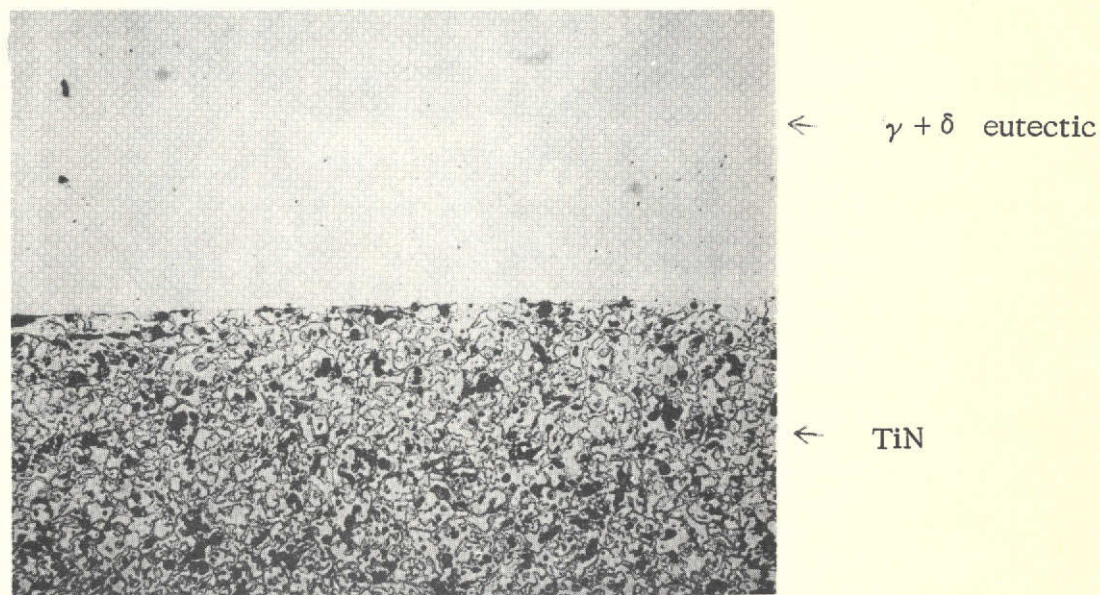
Fig. 5. TiN versus $\gamma + \delta$ alloy after 5-hr soak test in Ar $+5\%$ H$_2$ (X 130) 1370°C

$\leftarrow \quad \gamma/\gamma' + \delta \quad$ alloy

$\leftarrow \quad$ TaC
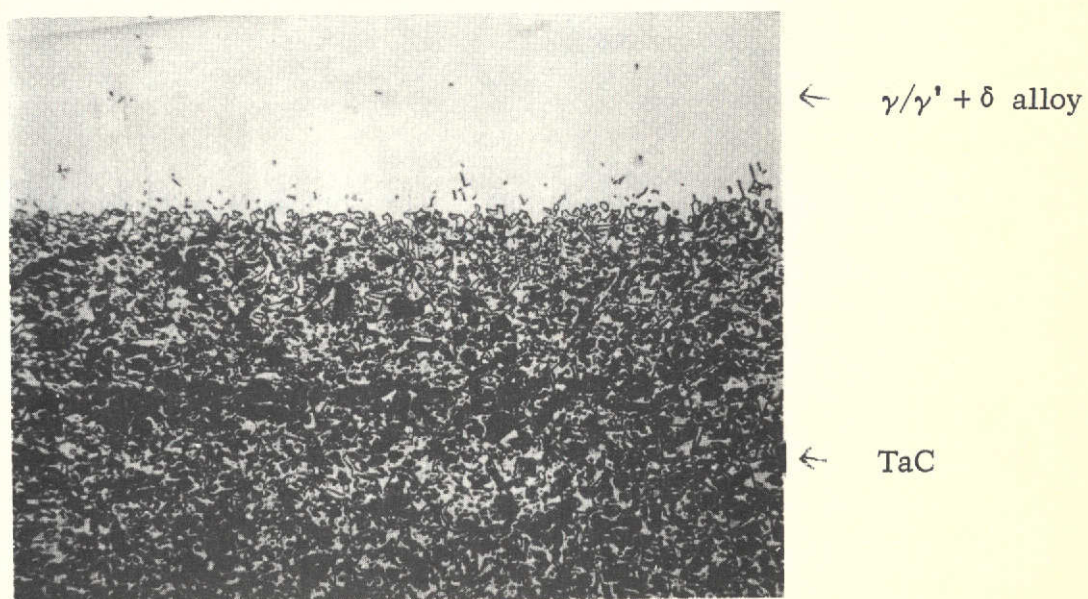
Fig. 6. TaC versus $\gamma/\gamma' + \delta$ alloy after 5-hr soak test in Ar $+5\%$ H$_2$ (X 130) 1380°C
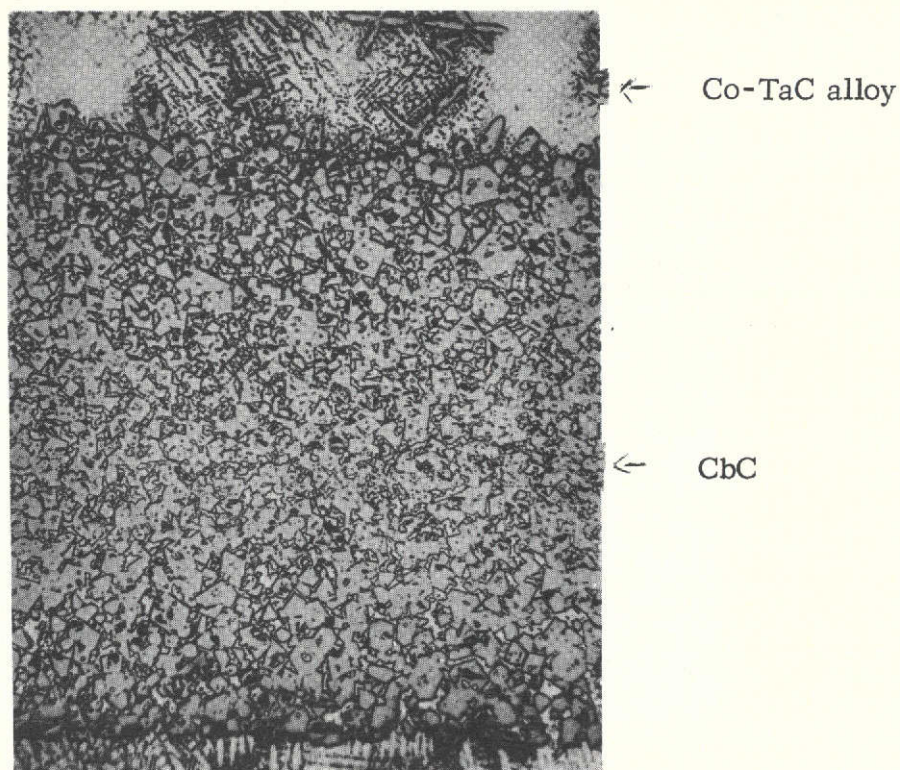
Fig. 7. CbC versus Co-TaC interface after 5-hr soak test (X 130) 1490°C

Table X. Contact Angle Measured on 1-hr Compatibility Samples (atmosphere Ar + 5% H$_2$). Tests were carried out with the respective alloys 100°C Superheated.

Ceramic \ Alloy	$\gamma + \delta$	$\gamma/\gamma' + \delta$	Co-TaC
TaC	~ 0°	15°, soaked in (2 samples)	~ 0°
TiN	33°	15°	20°
NbC	soaked in	14°	12°
HfC	20°	< 20°	~ 20°
W	0°	N.A.	N.A.
C	15°	N.A.	N.A.

conclusions based on wetting and soak tests and in order to finalize the choice of die materials for the remainder of the program. The primary emphasis of this work was to show that one or more die materials could be used to grow the three eutectic alloys. Table XI lists the growth runs carried out with this aim and indicate the problem areas identified as the work progressed.

The first two growth trials in Table XI were attempted using a thin, ribbon die TiO_2-10 TiC (Fig. 4d). The temperature was increased until the material in the crucible was molten. However, despite attempts to melt back the seed, the liquid could not be induced to rise in the capillary. Subsequently, the setup was taken apart and examined. The metal was found to be heavily coated with a black skin. The die itself had degraded to a powdery consistency.

In an effort to determine if a lower concentration of TiC in the die might eliminate this apparent interaction, a TiO_2-5% TiC substrate was heated in contact with the same alloy. The effect on the metal was the same. Next, the same substrate was heated in contact with the Co-TaC alloy. Again, it was observed that the alloy formed a dark skin and did not wet the die, while the die itself continued to degrade in integrity. It was concluded that this mixture of materials was unstable in the required temperature range.

Next a TaC die resembling the thin die (Fig. 4d) was prepared. This die did not taper at the top and was also raised in the setup to be nearly even with the top heat shield. The liquid ($\gamma + \delta$) alloy was found to rise readily in the TaC die. Seeding and growth were accomplished with little problem. The run failed however, as the result of fracture of one half of the top of the die. Material grown before die failure exhibited aligned structure at speeds of the order of 1 to 2 cm/hr.

Three runs, 707-106, 107, and 108 were carried out using the 0.38 cm tungsten rod-type die. In the first run, the die top was again positioned even with the top heat shield. Liquid again rose readily and seeding and growth were accomplished. The appearance of the solid-liquid interface was mushy, however, and the subsequent run was carried out with a new die raised 0.05 cm above the heat shield. That change was sufficient to make the interface appear sharp.

With the change in orifice height, control of the solidification rate became more satisfactory and it was found that rates of growth as high as 70 cm/hr could be achieved. The microstructures were in no cases completely lamellar, however. Size control was also difficult as the result of a lack of temperature control.

Table XI. Summary of Trial Growth Runs

Run No.	Alloy	Die Material	Comments
707-97	$\gamma + \delta$	TiO_2-10 TiC	No metal feeding; no growth
707-98	$\gamma + \delta$	TiO_2-10 TiC	No metal feeding; no growth
707-101	$\gamma + \delta$	TaC	Die broke during run; 7 cm grown. Die top just below heat shield
707-106	$\gamma + \delta$	W	Mushy growth; die top even with heat shield.
707-107	$\gamma + \delta$	W	Die top above shield, 16.5 cm grown
707-108	$\gamma + \delta$	W	Orifice failed
707-111	$\gamma + \delta$	Poco	No feeding; die just above die holder
707-117	$\gamma + \delta$	Poco	Poor feeding; discontinuous growth. Die below heat shield
707-118	$\gamma + \delta$	Poco	Die lowered, same result
707-120	$\gamma + \delta$	Poco	Die lowered, same result
707-121	$\gamma + \delta$	TaC	Die well below heat shield; 26 cm grown
707-122	$\gamma + \delta$	TaC	Metal flooded shields
707-125	$\gamma + \delta$	TaC	Seed broke after 11 cm grown
707-127	$\gamma + \delta$	TaC	24 cm grown
707-129	$\gamma + \delta$	TaC	rf coil adjusted; 10 cm grown
707-130	$\gamma + \delta$	TaC	Afterheater used; 9 cm grown
707-131	$\gamma + \delta$	CbC	Rapid die erosion; 11 cm grown
707-132	$\gamma + \delta$	Poco Graphite	No feeding; die above shield
707-133	$\gamma + \delta$	Poco Graphite	No feeding; die above shield
707-136	Co-TaC	TaC	rf set overloaded; 1.5 cm grown
707-137	Co-TaC	TaC	7 cm grown
707-141	$\gamma/\gamma' + \delta$	TaC	30.5 cm grown; poor spreading
707-143	$\gamma/\gamma' + \delta$	TaC	Coil adjusted; poor spreading 5 cm grown
707-144	$\gamma/\gamma' + \delta$	TaC	$\gamma + \delta$ seed used; 14 cm grown
707-148	$\gamma/\gamma' + \delta$	TaC	Air leak ruined setup
707-149	$\gamma/\gamma' + \delta$	TaC	9 cm grown; poor shape control
707-152	$\gamma/\gamma' + \delta$	TaC	11 cm grown; poor shape control
747-2	$\gamma/\gamma' + \delta$	TaC	3 cm grown; aligned structure
747-30	$\gamma/\gamma' + \delta$	HfC	1 cm grown; poor feeding
747-31	$\gamma/\gamma' + \delta$	HfC	1 cm grown; poor feeding

Fig. 8 compares section size variations in samples 707-101 grown from a TaC die and -107 grown from a W die. The essential points are that in both cases size control was difficult. In the case of sample -101, however, size control was maintained after the die broke. Shape control was somewhat easier to maintain in the sample grown from the metal die (-107).

The tungsten die interacted with the metal more rapidly than the tantalum carbide die. Further, the interaction was of a different kind. A sample of $\gamma + \delta$ in contact with tungsten was found to contain 11 wt % W after one hour exposure. A sample of the same alloy in contact with TaC was found to contain only 37 ppm of Ta, implying the lack of chemical dissolution.

We subsequently carried out several attempted growth runs (Nos. 707-111 to -120, and later -133 and -137) utilizing thin ribbon dies (-111 to -120) and the 0.120 cm rod type die of Poco graphite in combination with the $\gamma + \delta$ alloy. In all cases, feeding could be obtained only with difficulty and only thread-like growths were possible when feeding could be attained. One additional run was attempted using a TiN die. No feeding at all could be attained here.

Seven growth runs were next carried out using TaC or CbC ribbon dies of the type shown in Fig. 5e. The first three of these runs were carried out using dies not having the sloping shoulders shown in the figure. During these runs the pulling speed was varied and changes in die position and rf coil position were made. In one run, a metal ring above the upper heat shield was utilized as an afterheater, in order to determine if shape control could be improved.

In these runs, liquid rose to the top of the die with no subsequent difficulties in feeding. Other setup variables in ranges investigated had only slight effects. Growth speed was a stronger variable, both on structure and control. Shape control remained a problem with typical size variations as shown in Fig. 8 . Growth speeds were allowed to vary between 1 and 18 cm/hr

Over the course of a growth run, the dies were found to deteriorate by removal of material from the surface. This resulted in dimensional changes of the growing ribbon due to the sloping shoulders on the die. Metallography of the growth samples revealed that blocky TaC particles were embedded in the structure, suggesting that the cause of deterioration was removal of grains rather than dissolution. In general, the die was considered usable for 6 to 9 hours.

A die that had been in use for 7 hrs was sectioned and is shown in Fig. 9 In part (a) of the figure, the section through one of the feed channels is shown.
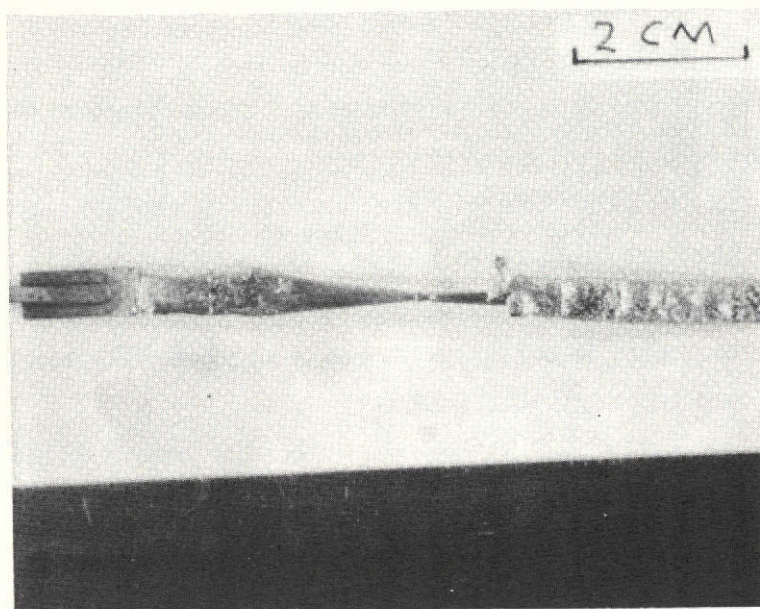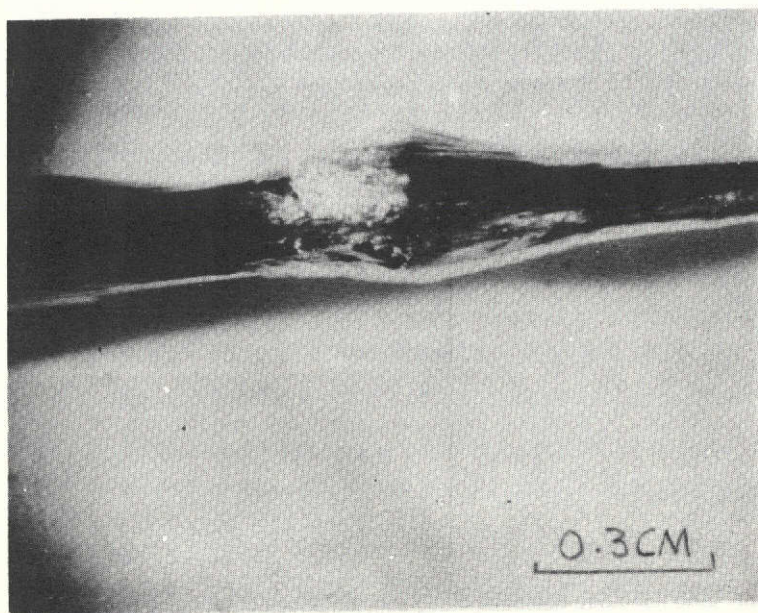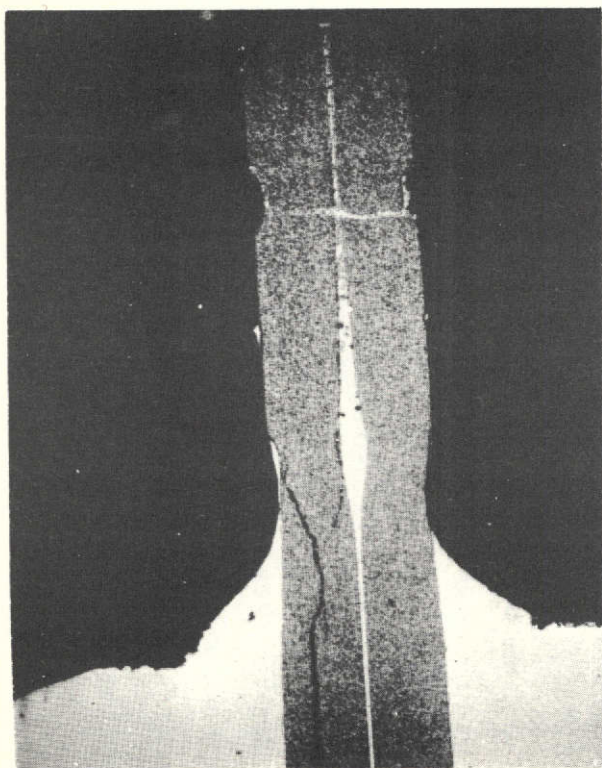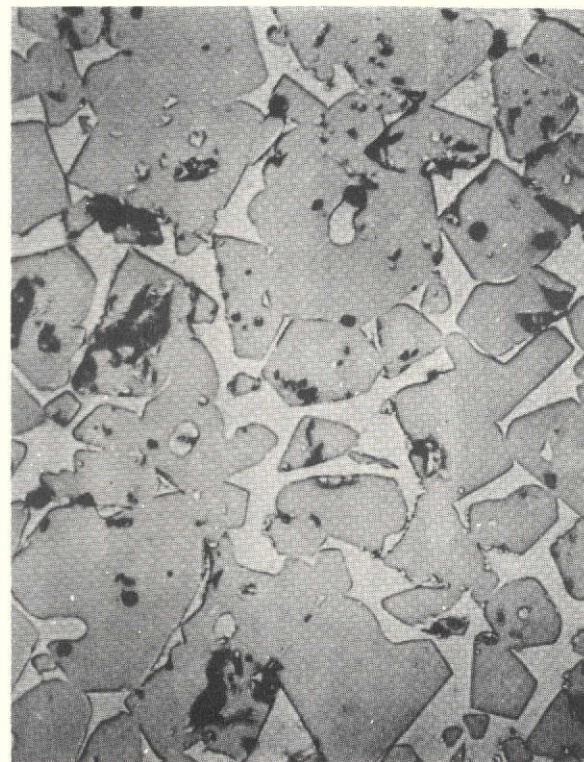
Fig. 8. Two early growth runs with the $\gamma + \delta$ alloy, (a) TaC die, Run No. 707-101, (b) W die, Run No. 707-107.

(a)

(b)

Fig. 9. Sections of TaC die; (a) Macrosection of TaC die after 7-hr of use (X 6),
(b) Microsection of TaC die after 7-hr of use showing grain boundary
penetration by the liquid $\gamma + \delta$ alloy (X 500)

Erosion at the top of the die is evident and also in the feed channel above the level of the meniscus formed by the metal in the crucible. This erosion in the feed channel is quite likely also due to particle erosion, suggested by the grains visible in the liquid above that point. Part (b) of the figure shows the microstructure of the die. Liquid has infiltrated the die body along the grain boundaries, an action made easier by the porosity.

We next turned to the cobalt base, tantalum carbide reinforced alloy. The setup used here was the same as that used for the $\gamma + \delta$ alloy with the die top 0.14 cm below the top of the uppermost heat shield. Two runs were carried out, resulting in two short ribbons being grown. No unusual difficulties were encountered.

Finally, we turned to the growth of the $\gamma/\gamma' + \delta$ alloy, again using the same type setup, but with the top of the die raised 0.038 cm. Growth trials with this configuration resulted in poor shape control and a mushy appearance to the growth interface. Difficulty with freezing to the die was encountered at growth speeds less than 3.8 cm/hr while speeds as low as 1.3 cm/hr were required to obtain a sharp interface.

At this time the setup was revised somewhat to attempt to obtain better thermal conditions. The changes incorporated were to lower the die by 0.038 cm while removing 0.056 cm from the crucible rim. These changes left the die top approximately 0.25 cm above the holding plate while bringing the top heat shield even lower relative to the die. In this way, the heat flow path from the holding plate was reduced while the thermal gradient was increased. These changes were effective and resulted in a satisfactory growth run (747-2).

HfC, despite wetting difficulties, had also appeared to show promise during the compatibility trials and was therefore briefly investigated. Two runs, 747-30 and -31, were carried out using HfC dies and the $\gamma/\gamma' + \delta$ alloy. The procedure adopted was to heat the setup under Ar to obtain wetting, then switch over to Ar + 5% H_2 to protect the sample from oxidation during growth. In both cases, however, only very short samples could be grown before feeding discontinued. Behavior during growth was satisfactory.

3.1.4 Microstructures

Metallography of samples grown during this die evaluation work was carried out in order to determine how fast samples could be grown with ordered structures without changes to the setup. These samples were ribbon samples with thicknesses

of the order of 0.05 to 0.10 cm. The ranges of growth speeds which had been achieved are listed in Table XII .

Table XII. Maximum and Minimum Growth Rates Achieved, cm/hr.

Die Material	$\gamma + \delta$	$\gamma/\gamma' + \delta$	Co-TaC
TaC (CbC)	18, 1	7.2, 1	6.4 , 1.8
W	71, 2.5	N. A.	N. A.
C	No growth	N. A.	N. A.
TiN	No growth	N. A.	N. A.
HfC	N. A.	3.8, 1.5	N. A.

Although growth of $\gamma + \delta$ was attempted from all but HfC of the die materials, no significant quantities were grown from any but TaC* and W. Also, it was found that although directional material was attained in both cases, aligned structures resulted only in the case of growth from TaC dies. The failure to produce aligned structures in the case of W dies was attributed to excessive dissolution of tungsten (11%), comparatively high rates of growth, and large section thickness (0.3 cm) .

During growth of $\gamma + \delta$, it was found that two external indications of the nature of the growth were observed. First, the appearance of the solid-liquid interface by its sharpness was found generally to indicate whether or not the material was aligned. Second, when fully aligned growth had been achieved, the surface of the as-grown sample exhibited striations.

The relationship of the external features to the structure of the alloy was determined by sectioning the alloy. Fig. 10a shows the surface of a sample where the growth speed had been changed from 1.5 to 5.4cm/hr. Figs. 10b and c show the transverse microstructure on either side of the speed change. The longitudinal

---

*During this investigation of $\gamma + \delta$, CbC was also used as a die material. No significant differences relative to TaC were noted.
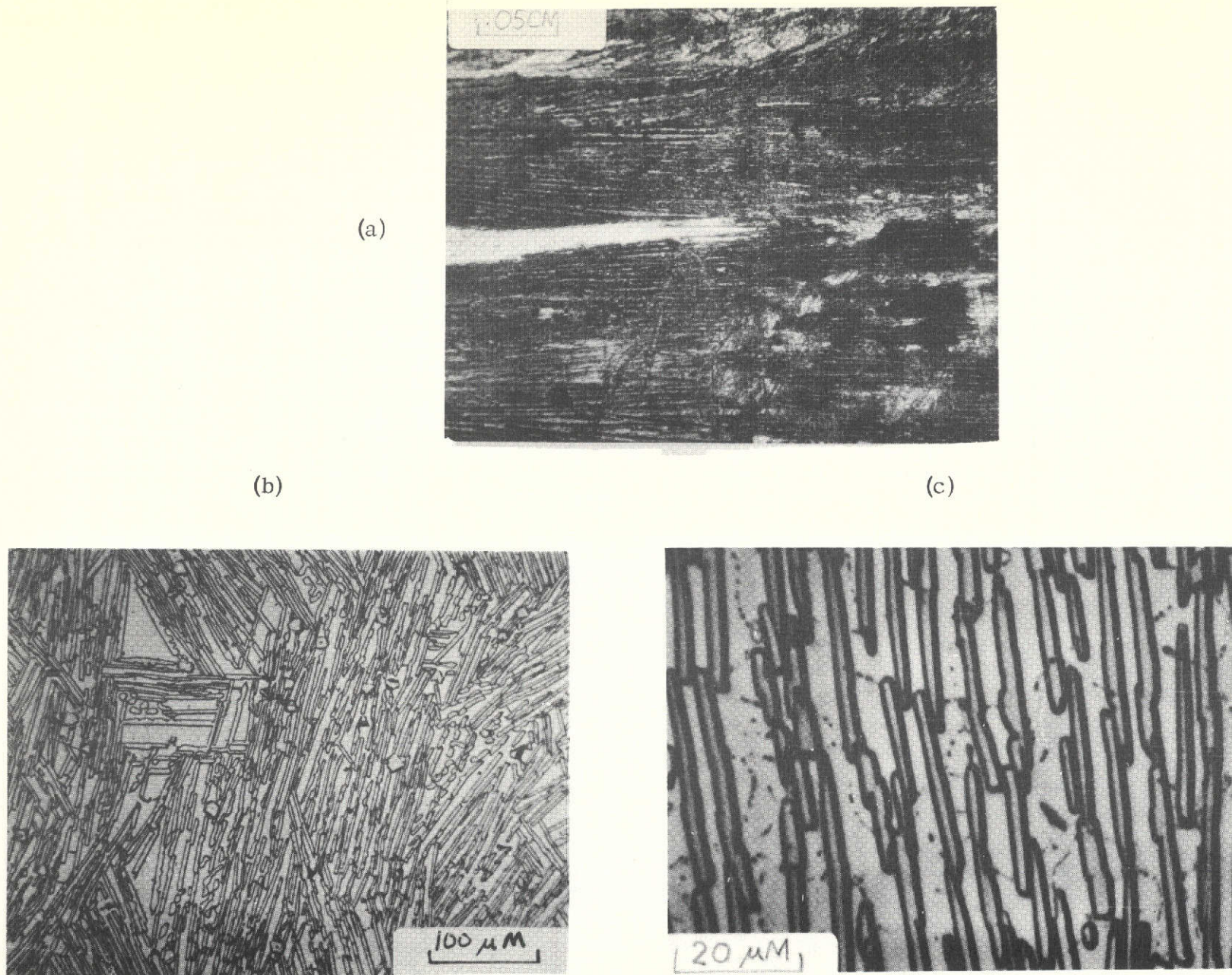
(a)

(b)

(c)

Fig. 10. Sections on both sides of a speed change in $\gamma + \delta$, (a) longitudinal sur-
face structure through speed change, and transverse section at (b)
1.5 cm/hr and (c) 5.4 cm/hr. Arrow indicates point of speed change

microstructure at 5.4 cm/hr is shown in Fig. 11. Surface striae indicating a lamellar microstructure were observed for growth speeds as high as 13 cm/hr as shown in Fig. 12. The interlamellar spacing was determined to be approximately 6.7 and 4.3 μm at 1.5 and 6.7 cm/hr respectively.

One sample of Co-TaC was grown incorporating a speed change from 1.8 to 6.1 cm/hr. This sample (707-137) was sectioned through the speed change and was found to undergo breakdown of the structure between these two speeds. Figs. 13a, b, and c show the longitudinal structure and the transverse structure at 1.8 and 6.1 cm/hr. The section grown at 1.8 cm/hr is fully aligned rods with no skin effect near the edge. The rod spacing was 3.10 μm at 1.8 cm/hr and 1.59 μm in the inter-dendritic material grown at 6.1 cm/hr in agreement with extrapolated data of Dunlevey and Wallace (ref. 3).

The early growth trials of the $\gamma/\gamma' + \delta$ alloy resulted in little aligned material. When the growth conditions had been properly adjusted, the appearance of the growth improved. Metallographic examination of sample No. 747-2 grown at 3.8 cm/hr showed the microstructure to be fully lamellar in the transverse section (Fig. 14). The alignment in the longitudinal section (Fig. 15) was exceptional. The microstructure in this case also appeared not to undergo any degradation with proximity to the surface. The interlamellar spacing was found to be 2.7 μm at 3.8 cm/hr.

3.2 Optimization of EFG Growth for $\gamma/\gamma' + \delta$

3.2.1 Gradient Studies

One aspect of the optimization of EFG growth is a determination of the gradient which is attained compared to theoretical. The procedure in carrying out this study was to use the bead of a chromel-alumel thermocouple as a seed to initiate some growth, then proceed to grow at a fixed rate while recording the output of the thermocouple by means of a strip chart recorder. The thermocouple was formed by the junction of two 0.07-cm dia wires and was meant to approximate the thermal configuration of the ribbon which is nominally 0.051-cm thick. Since the junction was of the order of 0.1 or more cm high, the initial temperature reading was expected to be (and was found to be) a few tens of °C lower than the alloy melting temperature.

The gradient was determined for setups using either $Mo + Al_2O_3$ (standard) holding plates, or pyrolytic graphite holding plates, and growth speed was varied from
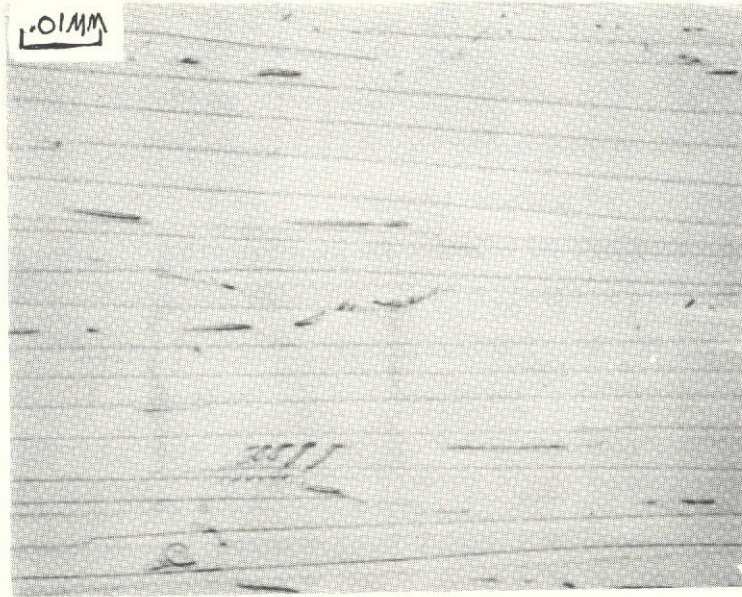
Fig. 11. Longitudinal section of $\gamma + \delta$ alloy grown at 5.4 cm/hr
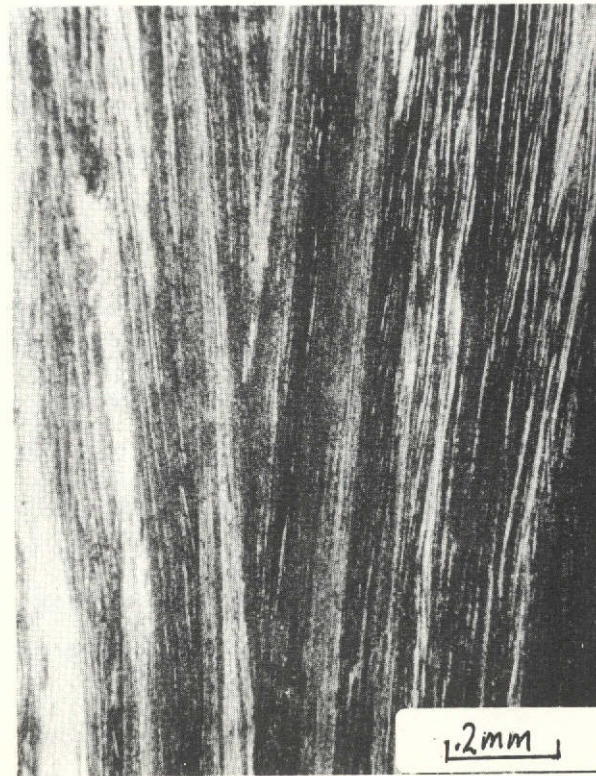
Fig. 12. Striae visible on surface of $\gamma + \delta$ grown from TaC die at 13 cm/hr
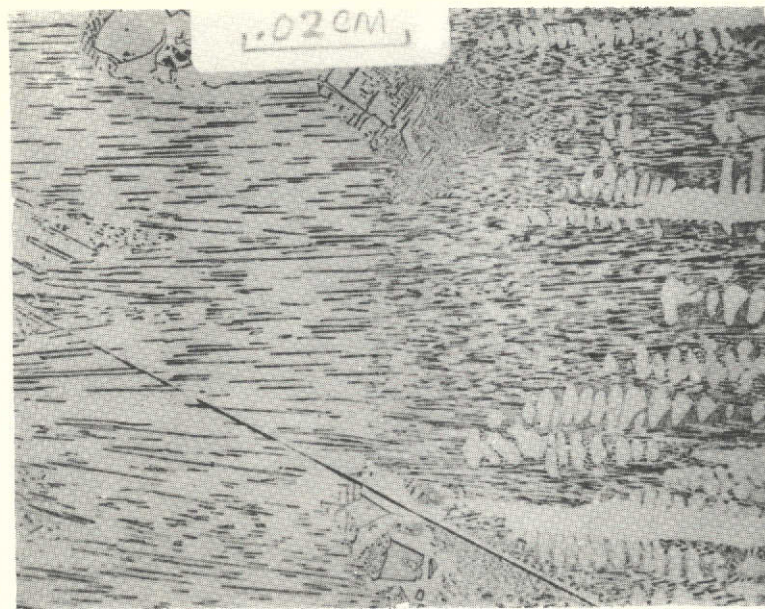
(a)

Speed change
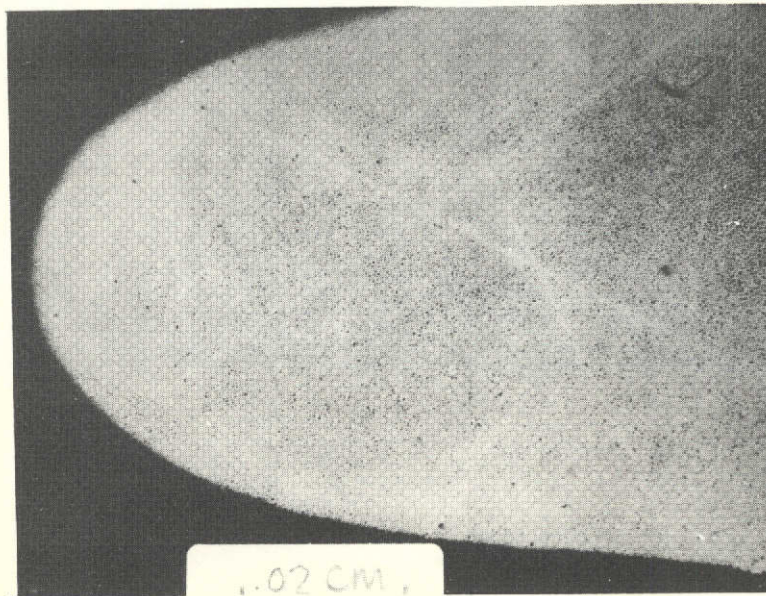
(b)
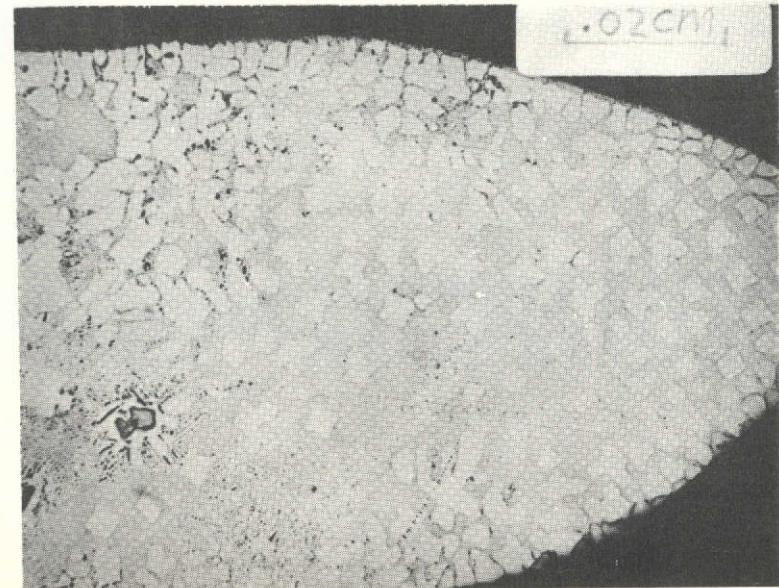
(c)

Fig. 13. Co-TaC alloy showing speed change from 1.8 to 6.1 cm/hr, (a) longitudinal structure through speed change and transverse structure at (b) 1.8 cm/hr and (c) 6.1 cm/hr. Arrow indicates speed change.
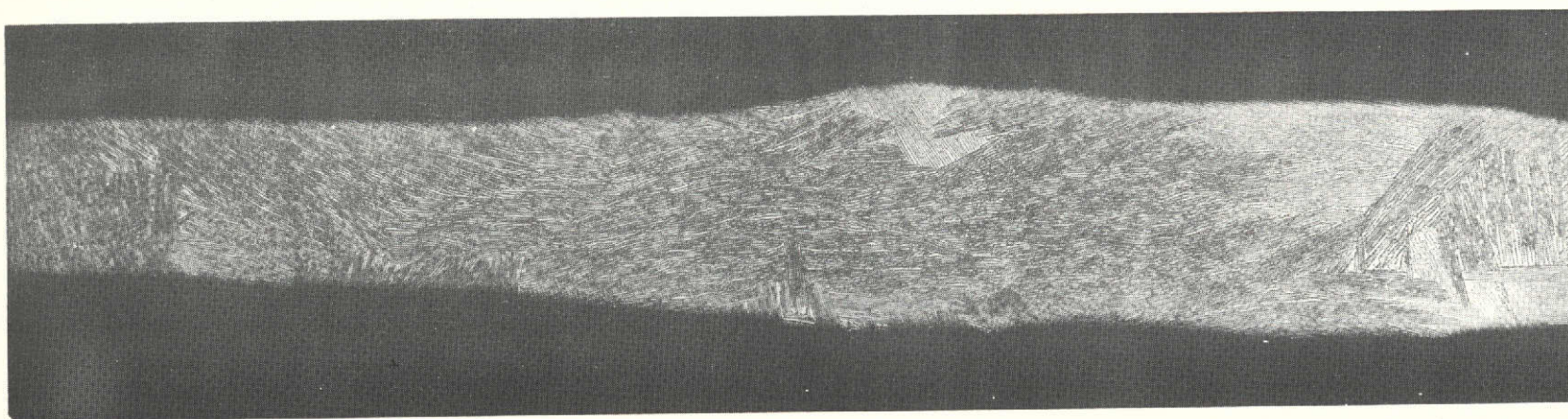
Fig. 14a. Transverse cross-section of $\gamma/\gamma' + \delta$ grown at 3.8 cm/hr (X 70)

Fig. 14b. Transverse cross-section of $\gamma/\gamma' + \delta$ grown at **3.8 cm/hr** (X 300)

Fig. 15. Longitudinal section of $\gamma/\gamma' + \delta$ grown at 7.6 cm/hr (X 70)

1.9 cm/hr to 7.9 cm/hr. The results are tabulated in Table XIII. When graphite holding plates were used, the gradient increased with the growth rate. Three results using $Mo + Al_2O_3$ holding plates gave scattered figures, including the sharpest gradient measured 923°C/cm. For comparison purposes, a theoretical gradient was calculated based on the assumption that lateral heat loss by radiation from the ribbon surface was the rate controlling step in determining the gradient. These calculations are presented in Appendix B.

3.2.2 Thin Ribbon Growth Rate

A series of growth runs was carried out to determine the fastest growth speed which was attainable with a fully aligned structure for the $\gamma/\gamma' + \delta$ alloy in the standard setup and to investigate the effect of more efficient heat transfer to the die on shape control and growth rate. These runs are listed in Table XIV.

Run 747-4 was carried out for the purpose of determining if the lamellar structure could be maintained at speeds of greater than 3.8 cm/hr. This sample was grown at 7.6 and 15 cm/hr. Results were that the structure became cellular - dendritic at 7.6 cm/hr (Fig. 15) and completely dendritic at 15 cm/hr.

Table XIII Thermal Gradient Study

No.	Holding Plate	Growth Speed (cm/hr)	Gradient (°C/cm)
747-7	Graphite	1.9	350
-12	$Mo-Al_2O_3$	4.4	923
-15	$Mo-Al_2O_3$	3.8	642
-17	$Mo-Al_2O_3$	7.9	610
-18	Graphite	3.6	498
-19	Graphite	3.8	517
-20	Graphite	3.8	530
-21	Graphite	7.9	687

Table XIV. Thin Ribbon Growth Runs with $\gamma/\gamma' + \delta$ and TaC Dies

Run No.	Configuration	Growth Rate (cm/hr)	Comments
747-4	Same as 747-2 (see p. 28)	7.62 - 15.2	Aligned, dendritic structure increasing with growth rate.
747-5	Pyrolytic graphite holding plates	3.8	Poor structure
747-23	Pyrolytic graphite holding plates	N. A.	Die failed
747-24	Pyrolytic graphite	N. A.	Solid mass atop die
747-25	P. G. + heavy top heat shield	N. A.	Would not spread
747-26	Mo + Al$_2$O$_3$ die holder + heavy top heat shield	3.8 - 7.62	Would not spread
747-27	Mo + Al$_2$O$_3$ die holder + heavy top heat shield	3.8 - 7.62	Would not spread
747-29	(see page 28)	3.8 + various	Aligned structure at 3.8 cm/hr.

The setup as used here differs from setups used for sapphire mainly in that the die itself is ceramic, and is therefore a comparatively poor thermal conductor, and also in that the die is coupled to the system by means of the alumina separators used in the die holding plate (Fig. 3). Thus the overall effect is that the conditions for holding the top of the die isothermal are probably not as favorable as in an all-metal system. One aid in overcoming this difficulty would be increasing the efficiency of thermal transport to the die from the holding plate. Pyrolytic graphite holding plates were fabricated and used to prepare growth setups. Three trials (runs 747-5, 23, and 24) were carried out in this manner with a wide range of growth speeds. None of the resulting structures was satisfactory.

During these runs, it was observed that solidification occurred on top of the die forming a skin and that liquid flowing up through the center froze above this skin. A new thick top heat shield designed to supply heat by radiation to the top of the die and meniscus was constructed as shown in Fig. 16. The edge of this piece, being wider and closer to the rf coil, is heated and transports heat inward toward the top of the die. The thick shield replaced the conventional heat shielding. Run 747-25 was carried out in this fashion. Some reduction in freezing of the skin was noted but the growth remained irregular. Since it now appeared that the graphite could not be tolerated in the system at all, the molybdenum and alumina holding plates were restored, and additional runs were carried out with the thick cap. These runs were also not successful. The setup was then restored to the standard configuration (747-2, p. 28) and confirmed that composite structure could be reproduced at 3.8 cm/hr.

3.2.3 Thick Ribbon Growth Runs

All previous ribbon growth runs had been carried out using ribbon dies which were 0.05 cm thick before eroding.* A new die configuration was designed in which the die remained 0.6 cm wide but was made 0.15 cm thick. Besides being more representative of a realistic section thickness, it was anticipated that this die might erode more slowly and lead to a smaller change in section size. These dies were combined with the standard setup using alumina spacers and molybdenum die holders.

Fourteen growth runs, listed in Table XV, were conducted using the thick ribbon dies and with the purposes of establishing the growth rate for plane front growth and of improving the shape control attainable. Growth rates of 0.6 to 18 cm/hr were achieved. Metallography showed that plane front growth was achieved for growth

---
*Fig. 4e.
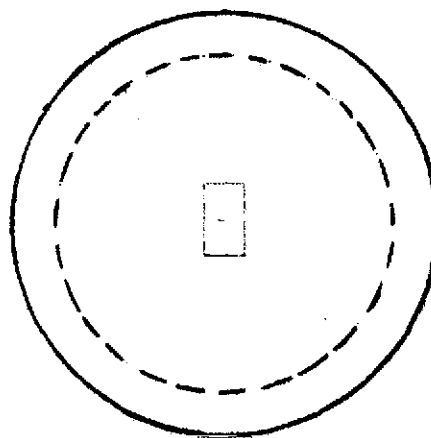
Fig. 16. Thick top heat shield

Table XV. Thick Ribbon Growth Runs with $\gamma/\gamma' + \delta$ and TaC Dies

Run No.	Configuration	Growth Rate (cm/hr)	Comments
747-33	Standard	3.8, 13	Fair shape control
747-35	Die slightly lower	13	Fair shape control
747-37	Same as -33	15	Fair shape control
747-38	Die closer to heat shield	12.7	Fair shape control
747-40	Same as -33	6.1, 15	Poor shape control
747-42	Same as -33	10, 15	Fair shape control
747-45	Same as -35	3.8, 7.6	Seed shifted
747-46	Standard	-	Die failed
747-47	Standard	15, 7.5, 3.8	-
747-48	Standard	3.8	Poor shape control
747-49	Standard	-	Die failed
747-50	Standard	0.64, 2.5, 7.5, 15	-
747-60	Standard	2.5	13 cm bar, good shape control
747-62	Standard	2.5	14 cm bar, good shape control

*In standard setup, die is approximately 0.13 cm below top heat shield.

rates up to 2.5 cm/hr. At faster rates of growth the structure remained directional but became dendritic. The structure for growth speeds of 0.64, 2.5, 12.5 and 15 cm/hr is compared in Figs. 17 to 19.

During all of the above runs, the parameters pulling speed and growth temperature were systematically varied to obtain their effect on structure. This made it difficult to obtain uniform dimensions in the bars grown. Two runs, the last two in Table XV, were carried out under constant growth conditions, resulting in two long bars of constant geometry. One of these bars is shown photographed in Fig. 20.

3.2.4 Effect of Helium Cooling

A simple arrangement for cooling the sample during growth was constructed and used for a single experiment, 747-52. This experiment utilized a standard ribbon die (0.15 × 0.6 cm, nominal) and standard setup other than the cooling arrangement. The latter was comprised of a glass tube arranged so as to direct a flow of helium from two directions onto the surface of the ribbon during growth. Growth rate was varied from 1.27 to 15.2 cm/hr. Reasonable dimensional stability was possible for growth speeds up to 7.62 cm/hr. The sample grown was 14.6 cm long and was distinguishable from the normal dull gray samples by having a bright straw-colored surface.

Sections of this sample which had been solidified at 1.3, 2.5, 3.8, 5.1 6.4, 7.6, and 15 cm/hr were metallographically examined. Inspection of trans-verse and longitudinal sections showed that the bar had substantially aligned structure for growth speeds up to 6.4 cm/hr. When no helium cooling was utilized, such structures, in 0.15 cm thick bars, were not attained at speeds above 2.5 to 3.8 cm/hr, Fig. 21a and b illustrate the breakdown of the structure in sample 747-52, when growth speed increased from 6.4 to 7.6 cm/hr.

At these growth speeds, using helium cooling, the element of die design was reflected in the structure of the bar. In simplest terms, the structure was best aligned where the bar grew above the solid portion of the die. Fig. 22 shows part of the transverse cross-section of the bar grown at 6.35 cm/hr. Fig. 23 illustrates the relationship of the structure to the die. It is concluded that this relationship is partly a function of die design and partly of the rudimentary nature of the cooling scheme. That is, more efficient cooling of the solid (rather than blowing gas at only one point) would help to eliminate the structural breakdown over the liquid.

44
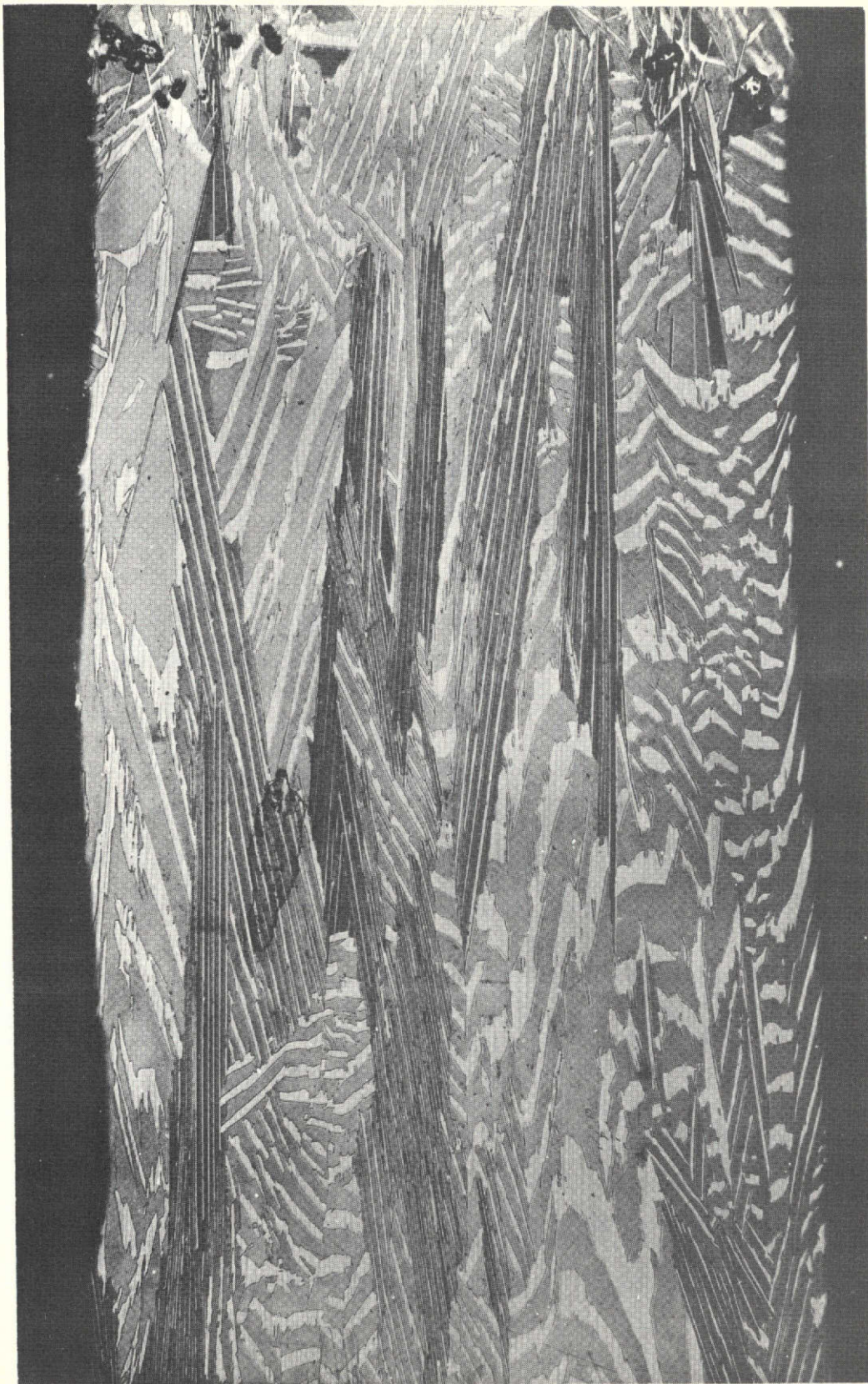
Fig. 17a. Microstructure of $\gamma/\gamma' + \delta$ grown at 0.64 cm/hr (747-50), (a) through-the-thickness.   Longitudinal section X 70. TaC particles from the die are evident at the top of the figure

Fig. 17b. Section perpendicular to (a). Longitudinal section (X 70)
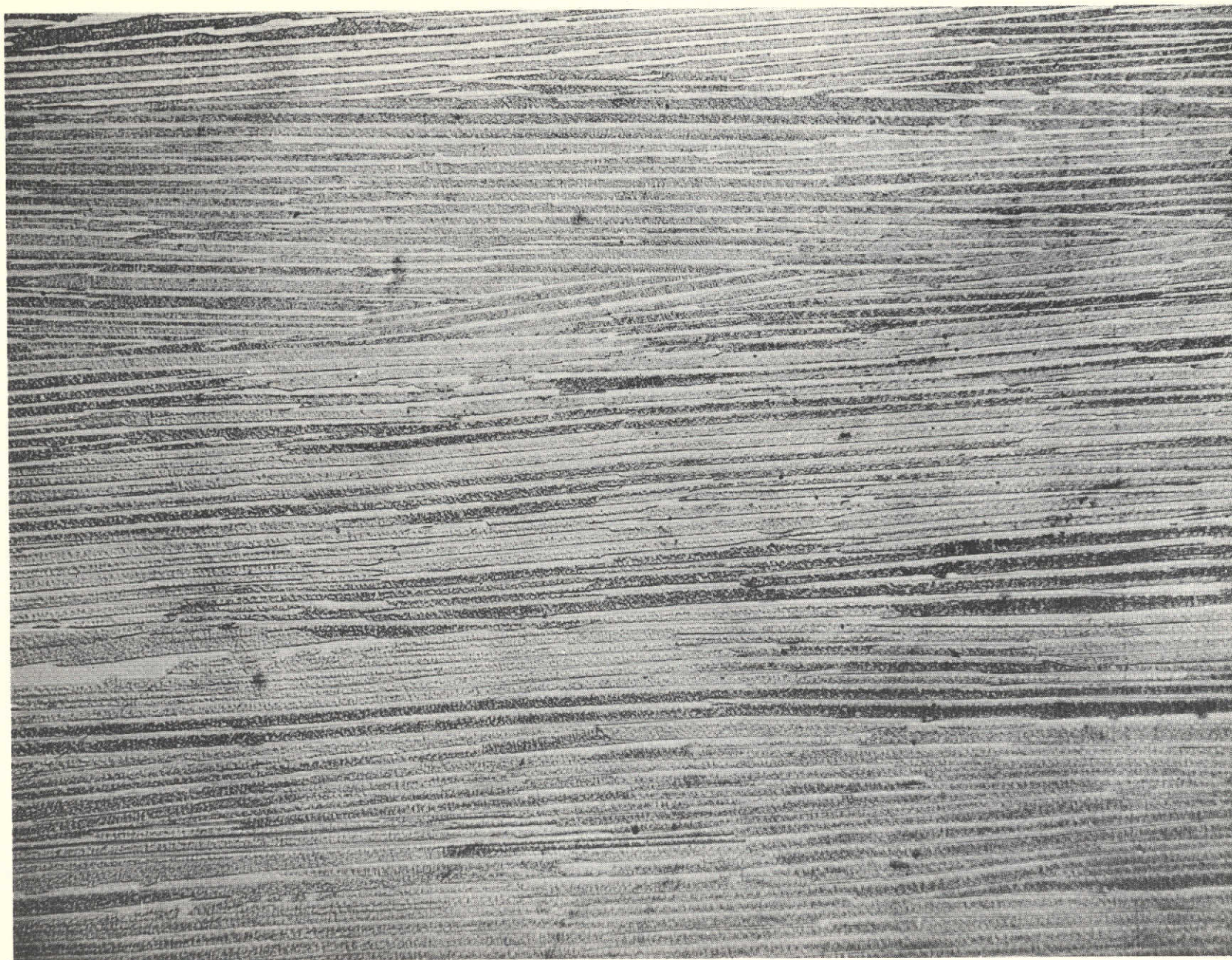
Fig. **17**c. Same as (b). Longitudinal section (X 300)

Fig. 17d. Transverse section (X 300)

Fig. 18a. Longitudinal sections at 90° to each other of $\gamma/\gamma' + \delta$ grown at 2.5 cm/hr, (747-50), (a) section parallel to broad face of ribbon (X 70)
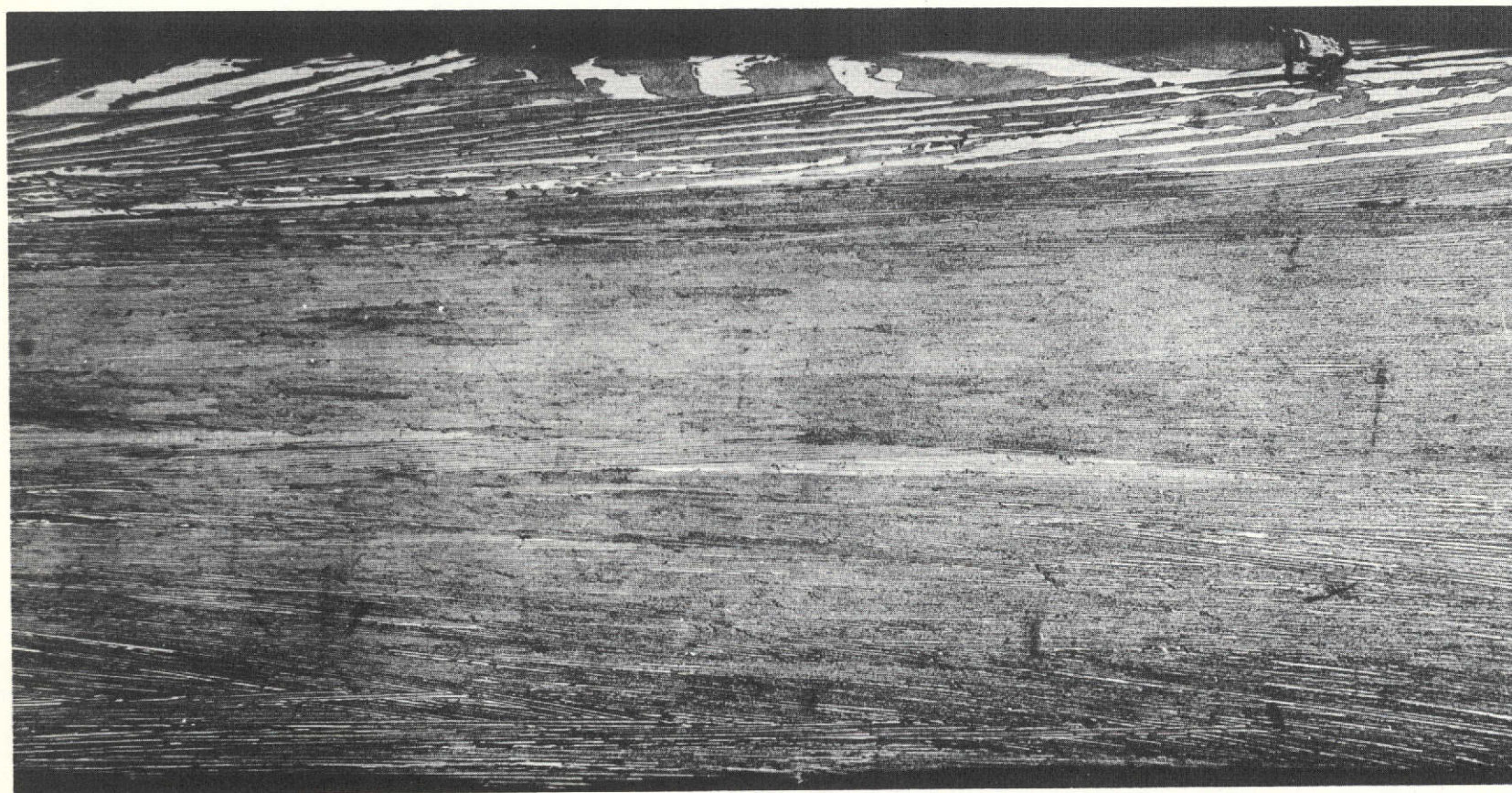
Fig. 18b. Section perpendicular to broad face, at center (X 70)

Fig. 18c. 2.5 cm/hr longitudinal section (X 260)

Fig. 18d. Transverse cross-section (X 300)
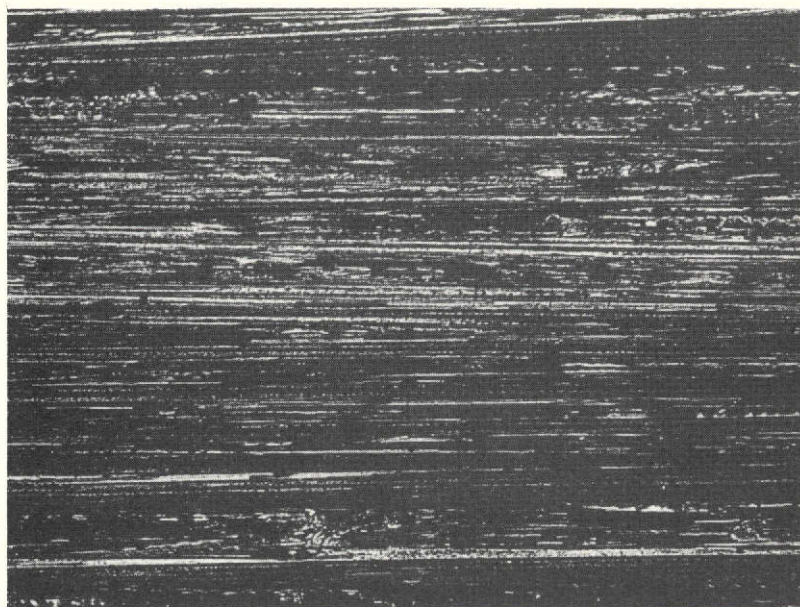
(a)
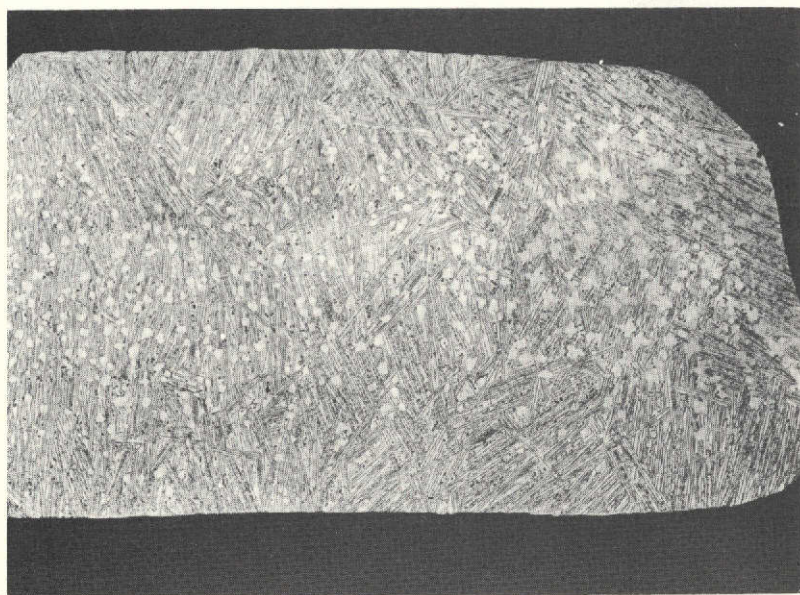
(b)

Fig. 19. Microstructure of $\gamma/\gamma' + \delta$ grown at speeds greater than 12.5 cm/hr, (a) Longitudinal section near surface of sample grown at 15 cm/hr (X 140); (b) transverse section of sample at 12.5 cm/hr. Note increased dendrite content at center (X 35) (747-50).
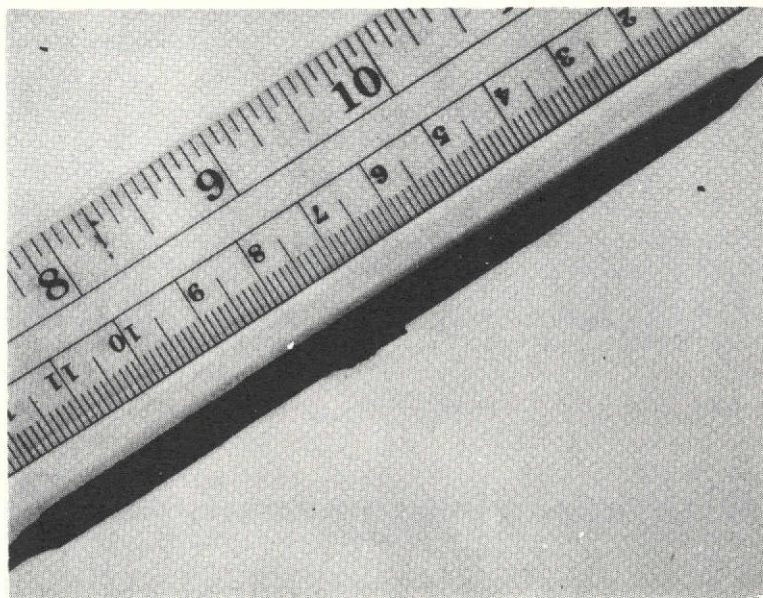
Fig. 20. Photograph of sample No. 747-60
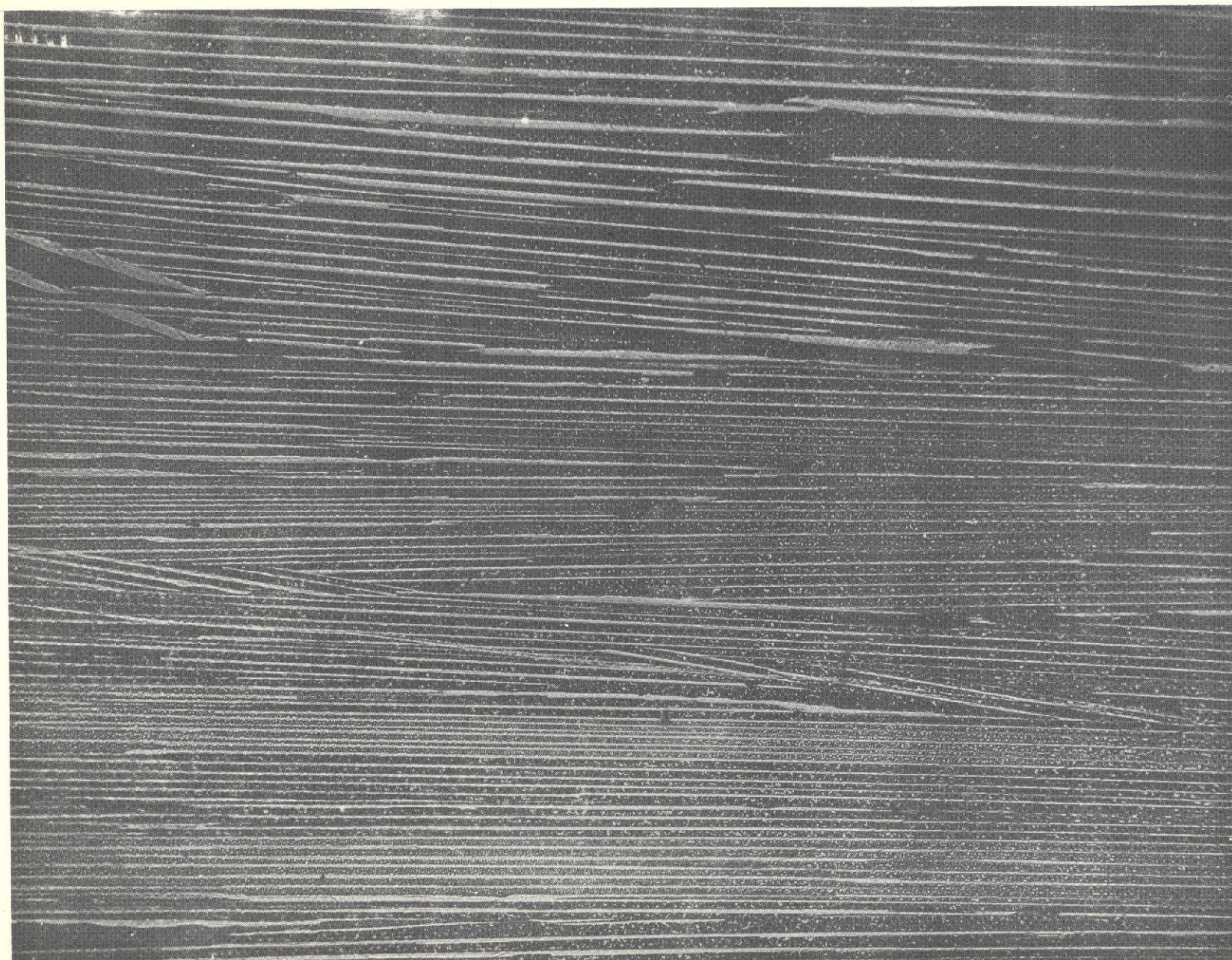
Fig. 21a. Longitudinal microstructure in sample of $\gamma/\gamma' + \delta$, 6.35 cm/hr
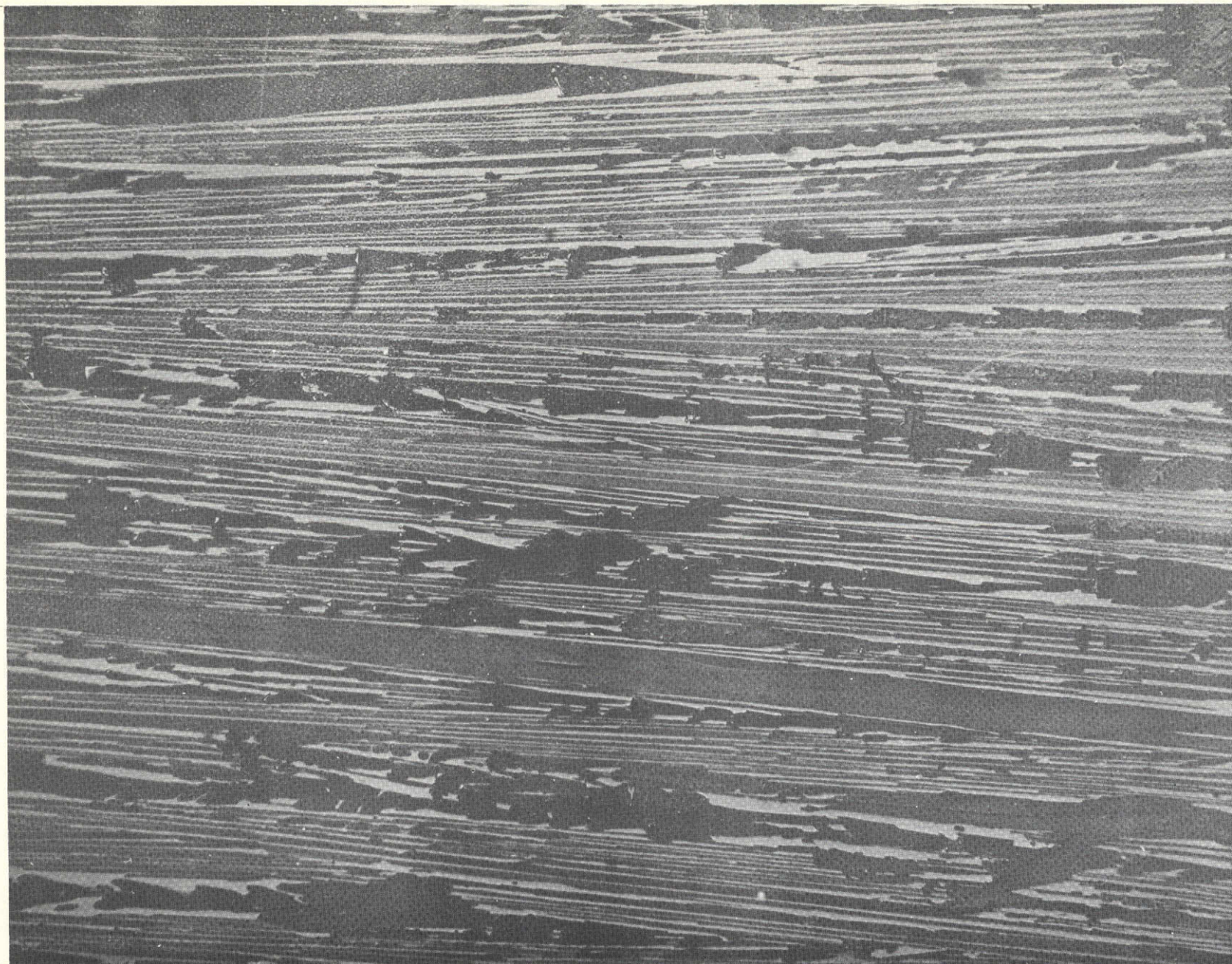
Fig. 21b. Longitudinal microstructure in sample of $\gamma/\gamma' + \delta$, 7.62 cm/hr (X 300)
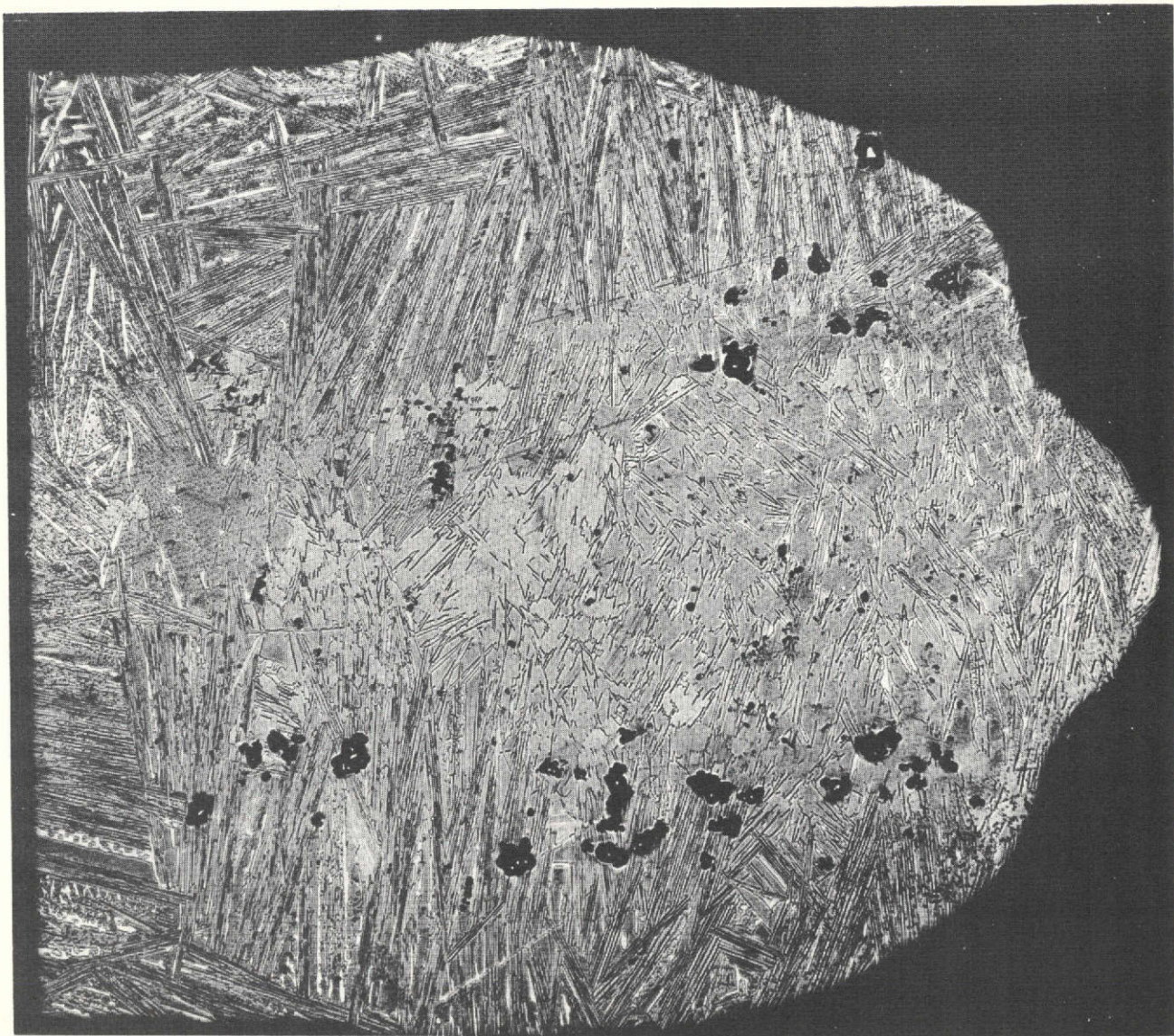
Fig. 22. Transverse microstructure in sample of $\gamma/\gamma' + \delta$ grown at 6.35 cm/hr, (X 110). Compare with schematic diagram in Fig. 23.
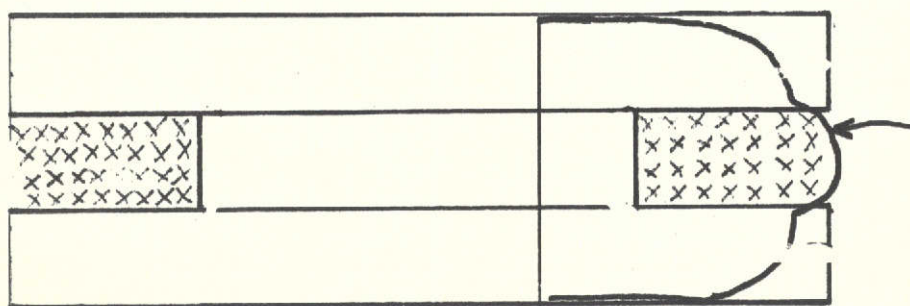
Area photographed in Fig. 22

⊠ — VERTICAL LIQUID FEED

Fig. 23. Relationship of structural degradation of die design

Area photographed in Fig. 22

3.2.5 Rod-Growth Experiments

The final series of experiments utilized circular rod-type orifices with diameters of 0.32, 0.48 and 0.64 cm. These orifices, Fig. 4e, were simply solid cylindrical rods of TaC with a longitudinal slot of 0.025 or 0.051 cm width cut along a radius. This series of experiments was attempted in order to determine the relationship between growth speed and section size in a simple geometry. The trials which were attempted are listed in Table XVI.

In the initial experiment, the feed slot was 0.051 cm in a 0.318 cm die. Difficulty in feeding was experienced. The subsequent experiment utilized a 0.025 cm feed slot in the same size die. Liquid rose to the top of the die and several short pieces were grown at 2.5 and 7.6 cm/hr. Feeding was erratic, and attempts to grow at slower speeds were unsuccessful.

Two more growth experiments were carried out using the 0.476 cm dia. die with four 0.025 cm wide slots spaced around the circumference. Feeding was better but attempts to stabilize growth at the necessary slow speeds were unsuccessful.

Table XVI. Rod Growth Runs with Slotted TaC Dies and $\gamma/\gamma' + \delta$

Run No.	Configuration	Comments
747-53	0.32 cm dia TaC, 0.05 cm die slot, die otherwise closely similar to standard ribbon setup	Difficulty in getting feeding; orifice broke up.
747-54	0.48 cm dia TaC die. 0.025 cm die slot, otherwise same as 747-53	Poor feeding, short erratic growth at 7.6 and 2.5 cm/hr
747-57	Same as 747-54	Same result - slightly better spreading.
747-57	0.48 cm dia TaC die, four 0.025 cm die slots	Better feeding. Ragged growth at slow speeds (< 2.5 cm/hr)
747-59	Same as 747-57	Would not spread

IV. CONCLUDING REMARKS

4.1 Die Materials

    The investigation of the die materials showed that several materials showed evidence of sufficient chemical compatibility to be used as die materials. In general, those materials having the largest (negative) heats of formation appeared the most stable and included the oxides and nitrides as well as HfC, TaC, and CbC. Borides in general were found to be quite reactive. Since judgments were made on the basis of microscopic examination of the one hour or, in a few cases, five hour compatibility samples, it could only be concluded that these combinations showed at least limited mutual compatibility. Experience was later gained in the use of alumina crucibles to contain each of the three melts and in attempting to use a TiN die in combination with the liquid $\gamma + \delta$ alloy. In these cases indeed the expectation of chemical compatibility was fulfilled.

    The tendency toward a particular die material being wetted was opposite to the tendency to be compatible. Thus, the oxides, nitrides, and carbides showed a tendency towards wetting in the order cited. Of these materials, the oxides showed wetting angles of the order of, or greater than, 90°, while the nitrides showed contact angles of 15 to 33°. The carbides CbC and TaC showed contact angles of 15° or less while HfC was similar, providing hydrogen (in the case of $\gamma/\gamma' + \delta$) was absent from the atmosphere. Capillary rise was observed only in the case of the carbides. This fact was surprising since calculations indicate that capillarity would be reduced only by about 16% when the contact angle is increased from 0° to 33°. Growth runs were conducted only when the liquid rose spontaneously in the die.

    Interactions between the die materials and the eutectic liquids were observed to be of four types. The oxides seemed not to interact at all, an ideal situation. In the case of the nitrides and of TaC and CbC, in combination with the liquid of $\gamma + \delta$ or

$\gamma/\gamma' + \delta$, the interaction was apparently slight and was usually marked by intergranular penetration of the liquid into the ceramic. Analysis of the $\gamma + \delta$ alloy confirmed that TaC had not dissolved in it to any significant extent. Tungsten and all of the borides tried were found to be significantly soluble in the liquid alloys. Analysis of a $\gamma + \delta$ sample grown from a tungsten die showed approximately 11 weight percent tungsten present. Boride-containing melts were not quantitatively analyzed but were qualitatively noted as being in this category. The final category was the group of materials which were found to react with a particular melt, forming a coating on the substrate. Two examples of this behavior were HfC with the Co-TaC alloy and carbon with $\gamma + \delta$. In both cases a carbide coating was formed on the ceramic. The formation of such surface interaction layers is not considered deleterious.

Final evaluation of several candidate die materials was carried out by growth trials. Materials from each of the above categories, except the non-interacting oxide materials, were tested. These trials showed that spontaneous capillary rise was observed only from dies fabricated of TaC, CbC, HfC, and tungsten. Graphite and TiN dies could be filled only by melting back the seed or other artificial means. This failure of spontaneous wetting to occur was surprising. However, it is of much greater importance that de-wetting does not occur once the die has been filled. Thus, while materials such as TiN would require a technique to obtain initial capillary rise, the surface tension would nevertheless be expected to operate to maintain shape control.

The final result of the die evaluation study was that TaC was selected to carry out the major portion of the growth trials. This material provided spontaneous capillary rise while maintaining chemical compatibility. This material, as well as other hot pressed ceramics, was found to be less than fully dense, and therefore, admitted liquid, spongelike, into the pores. Due to a low dihedral angle, grains were separated from the ceramic and resulted in erosion of the die in use. Individual hot pressed TaC discs had densities in the 85 to 92% of theoretical density range and yielded die lives of 6 to 8 hrs of continuous running. No firm correlation between density and die life was established but it was concluded that densities greater than 92% would have been required for a conclusive test.

Several avenues of approach could profitably be followed for future work on die materials. TaC is satisfactory but for the erosion of blocky carbide grains into the eutectic structure. The effect of carbide structure (grain size and density), on

60

this problem has not been determined. HfC is the second carbide material with potential applicability, especially for the monocarbide reinforced alloy. In this case, growth trials would be required to establish the effect on the growth behavior of the TaC - HfC interaction on the die surface.

The nitrides of the Group IV B metals also represent potentially useful die materials. TiN was partly investigated and gave promising results. ZrN and HfN which were not investigated represent choices of even greater thermodynamic stability and higher melting temperature. It is likely that all of these materials would require artificial die filling techniques but would exhibit contact angles substantially less than 90°.

Oxide materials may represent the best long range choice for the die materials with the best possible combination of long life and satisfactory compatibility. Both oxides investigated in this program were found to be nonwetting (i.e., $\gtrsim 90°$). However, preliminary indications are that oxides such as Cr_2O_3 are wetted with contact angles less than 90°. Further, $\gamma/\gamma' + \delta$ melts which were held in Al_2O_3 crucibles developed a scalloped interface along the periphery of the crucible with the contact angle alternately greater or less than 90°. It therefore seems quite likely that oxides or oxide alloys could be found which exhibited satisfactory contact angles. It would be expected that gas pressure would be used to fill such dies, a technique we have investigated in another system.

4.2 Growth Trials

Growth experiments were carried out and established that each of the three eutectic alloys could be grown by EFG utilizing TaC dies. Several general comments can be made based on these growth trials. First, in several important respects, the growth of the metal eutectics resembled that of other ceramic materials which we have grown. Thus, with the fully wetted die material, the melt was found to rise in the die feed slot so that establishing seed contact with the liquid was not a problem. The size and shape of the seed was found to bear no relation to the size and shape of the crystal grown so that a complicated seed would not be required to grow a shape. Unlike the growth of ceramic systems, changing setup configuration, growth speed, or temperature could often be seen to affect the interface resulting in mushy, fibrous, or sharp appearance of the interface. Due to the lower thermal conductivity of the TaC die and Al_2O_3 spacers compared with standard metal parts used, for example, in sapphire growth, some differences in the spreading behavior of the

liquid on the die top were noted. Thus the effect of high thermal conductivity in the metal assemblies is to make the die tend to be isothermal on top so that simple temperature adjustments can be made to obtain full spreading of the liquid. This condition was found to be more difficult to reach in the present case. Nevertheless, use of appropriate shielding and more careful (manual) temperature control made it possible to obtain regular geometries.

Since the vertical alignment and magnitude of the temperature gradient are most critical in the growth of eutectic composites, comments on the progress with these important variables are in order. Calculation of the gradient in the solid at the interface (see Appendix A) showed that if heat transfer at the surface of the sample by radiation to the environment were the rate limiting step, then a ribbon sample 0.1 cm thick should be able to exhibit a gradient of the order of 700°C/cm This value is in quite reasonable agreement with the range of values found by direct gradient measurements using a thermocouple seed (Table XIII).

A second method for experimental gradient determination is by calculation based on the critical G/R ratio and the maximum growth speed. Dunlevey and Wallace (ref. 3) report growth of the Co-TaC alloy in a furnace having a 90°C/cm gradient at 0.7 and 3 cm/hr. On this basis, our gradient would lie between 55 and 198°C/cm. The minimum gradient to growth rate ratio for the $\gamma/\gamma' + \delta$ alloy is calculated from (ref. 4) to be 40°C hr/cm^2. Our maximum growth rate for planar front solidification of this alloy was 3.8 cm/hr giving a gradient of at least 152°C/cm. Thus, the gradient for the uncooled apparatus is of the order of 152 to 198°C/cm, and falls short by about 2/3 of the calculated value. The experiment utilizing a primitive helium cooling device in this program indicated that substantial improvements in growth rate can be attained, in this case 6.3 cm/hr and 254°C/cm respectively. By comparison, conventional Bridgman solidification of this alloy yields plane front solidification breakdown at 1.3 to 2.5 cm/hr (ref. 5) while the most advanced and optimized Bridgman would seem to permit planar front solidification rates of 7.5 cm/hr.

Several reasons for gradient limitation in the present instance can be stated. First, the calculated gradient, besides assuming values for critical parameters such as surface emissivity which could be in error, was based on the dual assumptions that heat was lost by radiation to a non-reradiating environment, and that thermal conductivity to the surface was not rate-limiting. The first of these assumptions is not

true since in all experiments with $\gamma/\gamma' + \delta$, the die top was positioned below the top heat shield, and at least part of the heat shield was hotter than the top of the die. Thus, raising the die and changing the configuration of the heat shield to make it a sink would both be effective means of improving the gradient. Use of chilling devices also appears to be a promising method of heat removal. In this case, heat could be removed both from the crystal and from the heat shield by the same gas flow. The method of chilling would be based on a chill placed around the growing crystal and a gas flow between the chill and the crystal.

VI. REFERENCES

1. "Directionally Solidified Composites," National Materials Advisory Board, Division of Engineering National Research Council, Pub. No. NMAB-301, Washington, D. C., April 1973.

2. P. W. Bridgman, "Method of Growing Large Single Crystals," Proc. Amer. Acad. of Arts and Sciences, 60 (1925) 307.

3. F. M. Dunlevey and J. F. Wallace, "The Effect of Thermal Cycling on the Structure and Properties of a Co, Cr, Ni-TaC Directionally Solidified Eutectic Composite," NASA CR-121249, Sept. 1973.

4. F. D. Lemkey, "Eutectic Superalloys Strengthened by δ, Ni$_3$Cb Lamellae and γ', Ni$_3$Al Precipitates," NASA CR-2278, Nov. 1973.

5. P. M. Curran and J. S. Erickson, "Directional Solidification of Ni$_3$Cb Reinforced Eutectic Turbine Blades, "Third Quarterly Progress Report on Contract N00019-73-C-0252, Jan. 1974.

APPENDIX A

Description of EFG Processing

APPENDIX A

DESCRIPTION OF EFG PROCESSING

The edge-defined, film-fed growth process (EFG) is a new method of crystal growth which has been developed by Tyco Laboratories, Inc. A most noteworthy characteristic of the EFG processing technique has been its adaptability to multiple and rapid growth modes which has resulted in its being competitive not only with other methods of crystal growth, but even with other standard methods of materials processing and fabrication.

The earliest crystal growth experiments which led to the development of this method were aimed at the development of a process to grow single crystal sapphire filaments. These experiments were successful and resulted in the production of high strength (refs. A1, A2) sapphire filaments more than 400 feet in length with diameters of about 10 mils. One of the important tasks in this work was the development of a system of size and shape control so that the filaments would be regularly and precisely shaped. Success in meeting this requirement was followed by recognition that the method we used to control shape had far more general applicability and could, in fact, be used to produce much more complicated shapes.

The operation of the EFG process depends in two ways on the behavior of liquid films on solids which they wet. First, capillary rise is used to transport liquid from the main reservoir to the top of a die; then the surface tension is used in another way to hold the liquid film at the edges of the die while crystal growth is carried out.

Consider a solid rod with a fine, axial capillary, placed vertically in a pot of a liquid which wets the solid. Under these conditions, the liquid will rise in the capillary a distance determined by its radius, the surface tension of the liquid, its contact angle on the solid, and its density. In the case of liquid metals, the distance that the liquid will rise, when the solid is wetted, has been observed to be of the order of 1 in. or greater when the capillary is of the order of a few tens of mils diameter. These relationships are shown in Fig. A1.

68
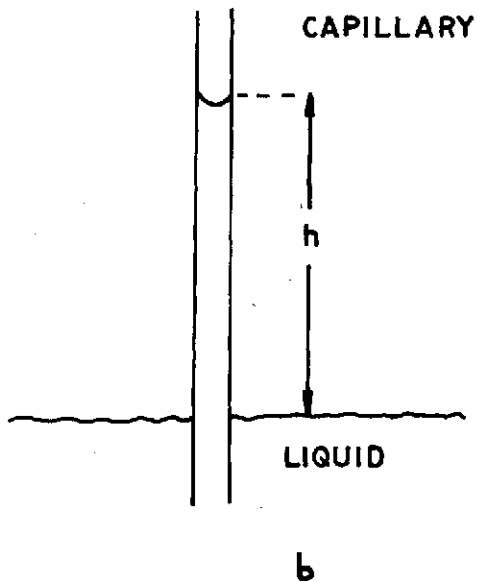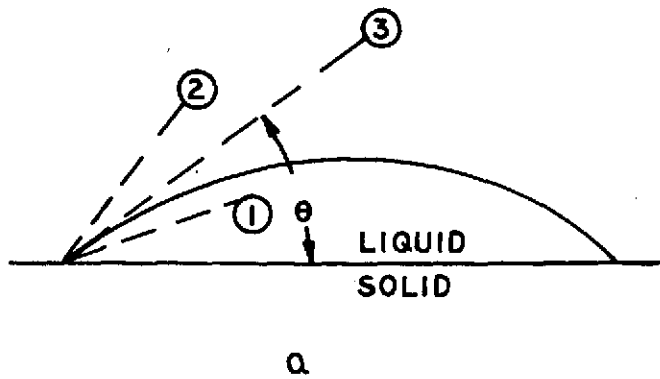
$$h = \frac{2 \gamma \cos \Theta}{\rho \, g \, r}$$

γ = surface tension

ρ = liquid density

g = 981 cm/sec^2

r = radius of capillary

Fig. A1. Behavior of liquids in contact with solids

    a. Liquid droplet on a solid which it wets. No. 3 shows equilibrium contact angle (liquid stationary); No. 1, liquid retreats; No. 2, liquid advances.

    b. Relationship between capillary rise, surface tension, and contact angle.

If the solid rod rises a distance above the liquid in the pot which is less than the distance that the liquid could rise, then the situation becomes as shown in Fig. A2 In Fig. A2, the liquid is shown having just risen to the top of the capillary in the rod. By itself, the liquid cannot flow over the edge of the capillary onto the top surface of the die, since the contact angle above the top surface would determine spreading (see Fig. A1a).

In Figs A2b through e, the necessary operations to cause the liquid to spread are shown. A solid seed of the same material as the liquid is dipped into the liquid. This seed is then withdrawn and the temperature is adjusted so that the liquid begins to freeze on the end of the seed. As the seed is withdrawn, the liquid is drawn upwards, as shown, so that the equilibrium contact angle on the top surface is exceeded. Now the liquid begins to spread, and as it does so, the solid growing from it also becomes wider. The liquid is ultimately bounded by the extreme edges of the die, since, once the liquid has spread that far, it cannot flow around the corner for the same reasons that it could not flow over the top edge of the capillary.

Thus, the size and shape of the growing crystal are controlled by the external dimensions of the top of the die. But additional controls are also possible. Consider the die shown in Fig. A3, for example. Here a capillary in a solid rod is again used to conduct liquid to the top die surface. In this case, however, the top die surface has been modified by a blind hole drilled into it. During seeding, the liquid will spread to this hole, but will stop at its edge since it cannot distinguish a blind hole from an outside edge. Thus, the crystal, which grows only above the liquid film, will grow with a hollow cavity above the blind hole, mirroring its cross-sectional shape.

Consideration of the mechanism described in the last section shows that the basic requirements for crystal growth by the EFG method are that the liquid must wet the die material without reacting with it. In a great many cases, these conditions are readily met, and we have applied this method of crystal growth to a large number of crystalline metals, alloys, ceramics, ceramic-alloys, and semiconductors. However, we have recently analyzed the situation which occurs when the contact angle shown in Fig. A1 is greater than zero. Our analysis, backed by some experimental work, is that zero, or close to zero contact angles are a convenience rather than a necessity for EFG growth. Thus size and shape control are possible in other than fully wetting systems.
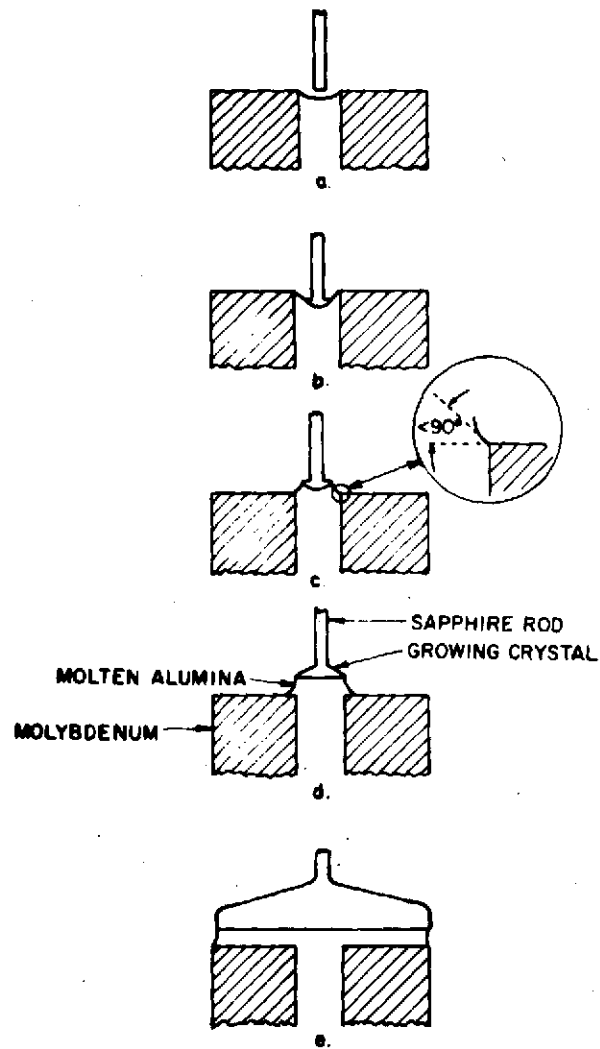
Fig. A2. Sequence of events during seeding

CONTINUOUS HOLE
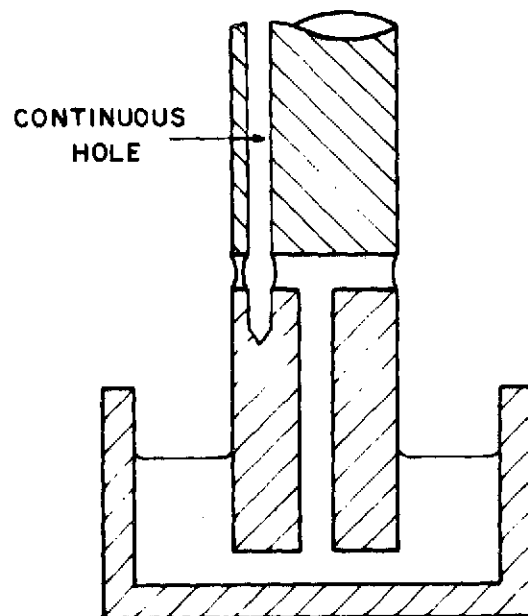
Fig. A3. Method of growing a cavity in a solid rod

REFERENCES

1.   H. E. LaBelle, Jr., "Growth of Controlled Profile Crystals from the Melt: Part II, Edge-Defined, Film-Fed Growth," Materials Research Bulletin, 6, (1971) 581.

2.   G. F. Hurley and J. T. A. Pollock, "Mechanical and Structural Characterization of Sapphire Ribbons and Continuous Filaments," Met. Trans. 3 (1972), 397.

APPENDIX B

Thermal Gradient - Limited by Radiative Heat Transfer

APPENDIX B

Thermal Gradient - Limited by Radiative Heat Transfer

The thermal gradient was calculated for two cases: that of a cylindrical crystal and that of a ribbon-shaped crystal. In both cases the assumption was made that radiative heat transfer from the surface was the rate limiting step in heat removal.

We begin by calculating the solid gradient which can be attained in a circular cross-section crystal based on the assumption that thermal conductivity, transversely in the crystal, does not limit the rate of heat removal. Fig. B-1 shows the heat flow in such a crystal. Attribution in the heat flow here is caused by radiative heat loss from the surface.

At steady state:

$$Q_1 - Q_2 = Q_R \tag{1}$$

Since axial heat flow at any given point is determined by the thermal gradient at that point, Q_1 or Q_2 can be found from

$$Q_i = -k\pi r^2 \left(\frac{dT}{dx}\right)_i \tag{2}$$

where k is the thermal conductivity of the solid. Also:

$$Q_R = 2\epsilon \sigma \pi r T^4 \Delta x \tag{3}$$

where ϵ is the emissivity of the surface and σ is the Stefan-Boltzmann constant.
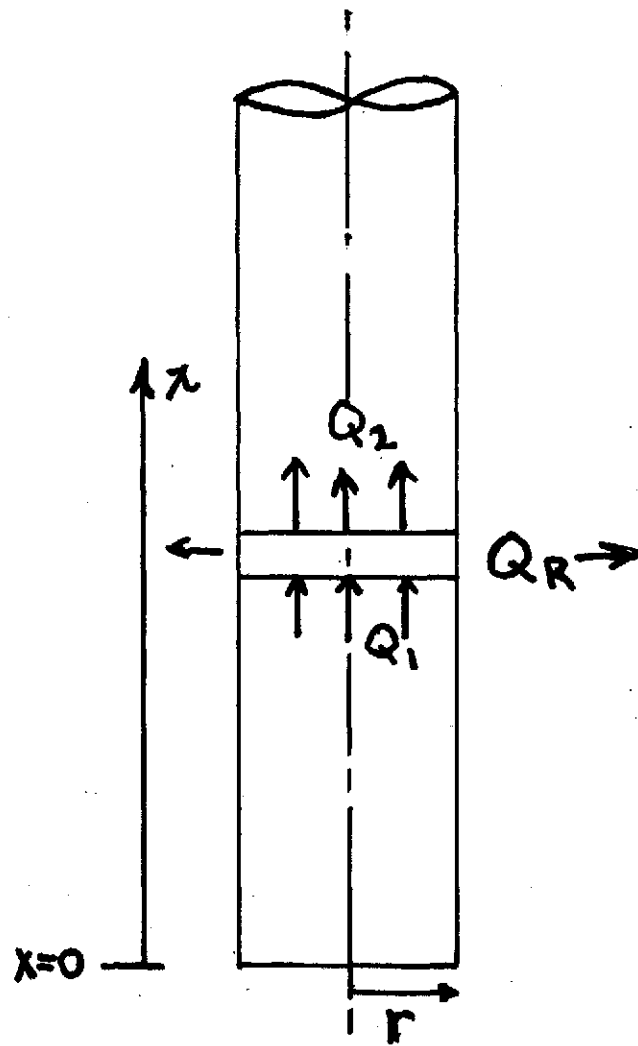
Fig. B1. Heat flow in solidifying rod

Equation (1) can now be restated as follows:

$$-kr \left[\left(\frac{dT}{dx} \right)_1 - \left(\frac{dT}{dx} \right)_2 \right] = 2\epsilon \, \sigma \, T^4 \, \Delta x \tag{4}$$

Since, by definition:

$$\lim_{\Delta x \to 0} \frac{\left[\left(\frac{dT}{dx} \right)_2 - \left(\frac{dT}{dx} \right)_1 \right]}{\Delta x} = \frac{d^2 T}{dx^2}$$

then:

$$\frac{d^2 T}{dx^2} = \frac{2\epsilon \, \sigma \, T^4}{kr} \tag{5}$$

This basic equation, (5), describes the temperature distribution in a rod under conditions where heat enters at one end and is lost to a non-reradiating environment along the sides.

Equation (5) can be integrated directly:

$$\frac{dT}{dx} = \pm \left[\frac{2AT^5}{5} + 2B \right]^{1/2} \tag{6}$$

where $A = \frac{2\epsilon \, \sigma}{kr}$ and B is the constant of integration. B is determined to be zero by the boundary condition that $\frac{dT}{dx} = 0$ when $T = 0$, and a minus sign is chosen to yield the proper direction of heat flow. Thus, the final expression for the gradient in the solid becomes:

$$\frac{dT}{dx} = - \left[\frac{2AT^5}{5} \right]^{1/2} \tag{7}$$

The next step to determine the gradient in the liquid as a function of the gradient in the solid is also a heat flow balance, at the solid-liquid interface. The gradient in the solid, Eq. (7), multiplied by the thermal conductivity represents the rate of heat transportted vertically through the solid at this interface. This differs from that in the liquid by the difference in thermal conductivity between liquid and solid, and by the latent heat of solidification. The thermal expression is:

78

$$k_s \left(\frac{dT}{dx}\right)_s = k_1 \left(\frac{dT}{dx}\right)_1 + L \cdot R \tag{8}$$

where subscripts s and l refer respectively to solid and liquid values. L is the latent heat of solidification, and R is the growth rate. This expression can then be rearranged to give $\left(\frac{dT}{dx}\right)_1$ as a function of $\left(\frac{dT}{dx}\right)_s$ and the growth .

Thus:

$$\frac{dT}{dx}\Big|_1 = \frac{1}{k_1} \left[k_s \frac{dT}{dx}\Big|_s - L \cdot R\right] \tag{9}$$

This equation has no unique numerical solution for $\left(\frac{dT}{dx}\right)_1$ since a value for R is not specified. In order to obtain a solution, one can plot $\left(\frac{dT}{dx}\right)_1$ versus R from Eq. (9) for a particular alloy and then find the intersection of this line with $\left(\frac{dT}{dx}\right)_1$ versus R from the relationship that $\left(\frac{dT}{dx}\right)_1 = \left(\frac{G}{R}\right)_{min} XR$, where G/R_{min} is a constant for any particular alloy.

Equation (9) has been evaluated for values of $\left(\frac{dT}{dx}\right)_1$ in two stages: first, by solving Eq. (7) for $\left(\frac{dT}{dx}\right)_s$ as a function of different values of r between 0.025 and 2.5 cm. These values were then used to calculate values of $\left(\frac{dT}{dx}\right)_1$ for several values of R between 3.53×10^{-4} and 70.6×10^{-4} cm/sec. Results of these several calculations are presented in the following tables B-1 and B-2. The physical constants used are listed in Table B-3.

We now go on to the case of the ribbon geometry which is more equivalent to the work described in this report. Fig. B-2 describes the heat flow in the case of a ribbon crystal with heat loss by radiation from the surface. Again, the heat balance is the same (Eq. 1), while the individual terms become:

$$Q_i = - kwt \left(\frac{dT}{dx}\right)_i \tag{10}$$

and

$$Q_R = 2\epsilon \sigma (w + t) T^4 \Delta x \tag{11}$$

79

Table B-1. Calculated Values $\left(\dfrac{dT}{dx}\right)_s$ for Rod Geometry

r (cm)	(dT/dx) s (°C/cm)
0.0254	1403
0.127	627
0.254	442
0.635	280
1.27	198
2.54	140

Table B-2. Calculated Values of $\left(\dfrac{dT}{dx}\right)_\ell$, °C/cm

R in./hr	R cm/sec	r = 0.0254	r = 0.127	r = 0.254	r = 0.635	r = 1.27	r = 2.54 cm
0.5	3.53×10^{-4}	2540	1130	792	497	360	242
1	7.06×10^{-4}	2530	1120	780	485	336	229
5	35.3×10^{-4}	2430	1010	676	381	232	125
10	70.6×10^{-4}	2300	883	546	251	102	< 0

Table B-3. Value of Physical Constants Used in Calculations

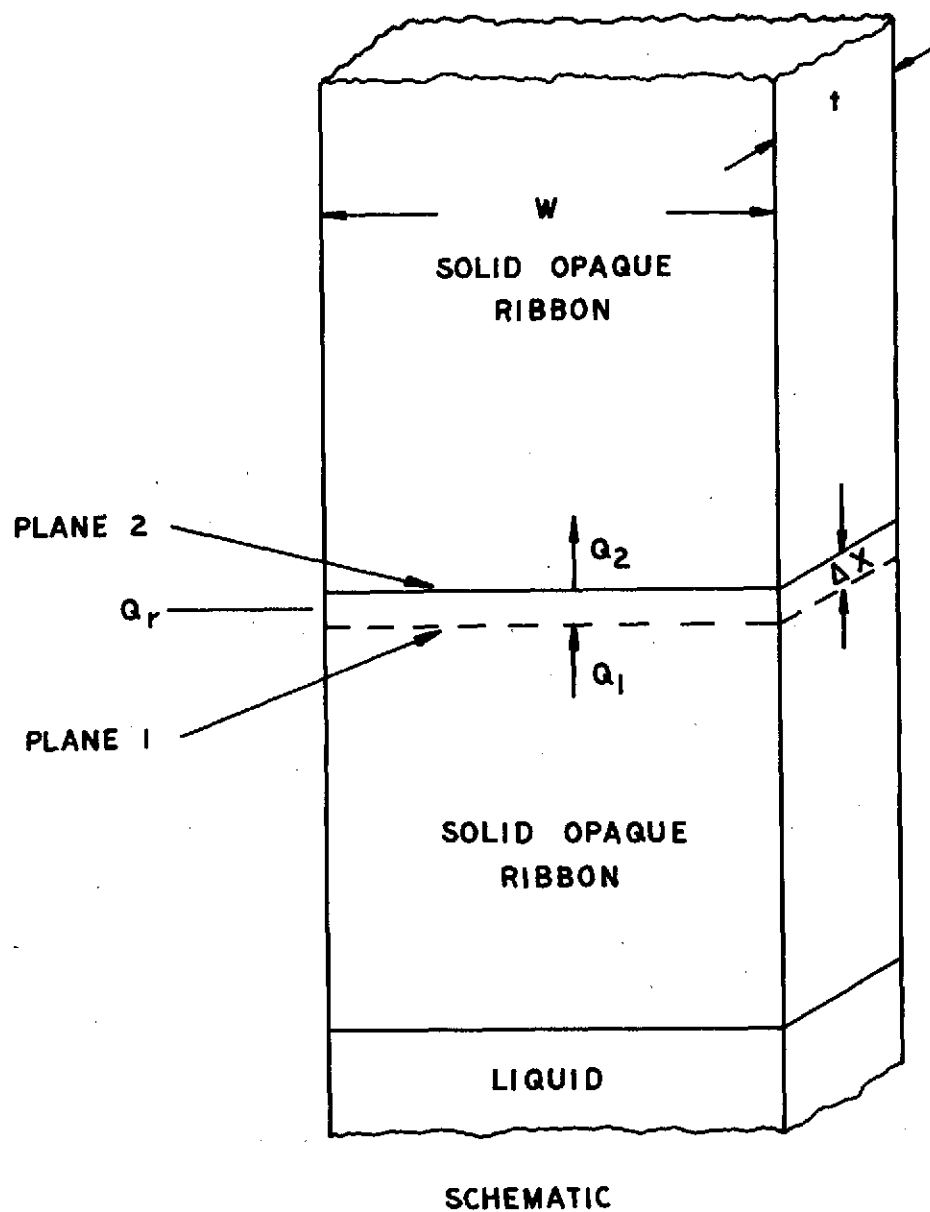| Constant	Value
ϵ	0.4
σ	1.355×10^{-12} cal/sec cm^2 °K^4
k_s	0.066 cal/sec cm °K
k_ℓ	0.036 cal/sec cm °K
L	157 g cal/g
Tm	1500 °K
ρ	8.49 gms/cm^3

Fig. B.2. Heat flow in an opaque, ribbon-shaped crystal

where w and t are the width and thickness of the ribbon and the other terms have been defined, Eq. 1 for the ribbon now becomes:

$$-\text{kwt} \left[\left(\frac{dT}{dx} \right)_1 - \left(\frac{dT}{dx} \right)_2 \right] = 2\epsilon \sigma \ (w + t) \ T^4 \ \Delta x \tag{12}$$

Whence, as before:

$$\frac{dT}{dx} = - \left[\frac{2MT^5}{5} \right]^{1/2} \tag{13}$$

where

$$M = 2\epsilon \sigma \ (w + t) \ / \ \text{kwt}$$

Eq. (13), which is the gradient in the solid, is calculated for various sizes of ribbons with the results listed in Table B-4. These results are used in Eq. (9), then, to obtain values of the gradient in the liquid. Those results are given as a function of growth speed and ribbon thickness in Table B-5. Since the ribbon geometry has a greater surface to volume ratio for a given cross-section area than a cylindrical rod, its predicted value of G_s should be greater. For example, a ribbon 0.05 × 1 cm has a cross-sectional area of 5×10^{-2} which is essentially the same as a rod, 0.127 cm radius. The calculated values of G_s for these two cases are 1020 and 627°C/cm, respectively.

Table B-4. Calculated Values of $\left(\dfrac{dT}{dx}\right)_s$ for Ribbon Geometry

W (cm)	t (cm)	$\left(\dfrac{dT}{dx}\right)_s$ °C/cm
0.6	0.05	1040
1.0	0.05	1020
1.0	0.05	1000
0.6	0.1	762
1.0	0.1	741
1.0	0.1	710
0.6	0.2	577
1.0	0.2	547
10	0.2	504
0.6	0.3	499
1.0	0.3	465
10	0.3	414
0.6	0.5	428
1.0	0.5	387
10.0	0.5	324

Table B-5. Calculated Values of $\left(\dfrac{dT}{dx}\right)_\ell$, °C/cm

R in./hr.	R cm/sec	Ribbon Dimensions, cm				
		0.05×1	0.1×1	0.2×1	0.3×1	0.5×1
0.5	3.53×10^{-4}	1850	1340	923	834	692
1.0	7.06×10^{-4}	1830	1320	910	821	687
5.0	35.3×10^{-4}	1730	1220	867	717	575
10.0	70.6×10^{-4}	1600	1090	737	587	445

DISTRIBUTION LIST

Mr. J. Acurio - MS 77-5
NASA Lewis Research Ctr.
21000 Brookpark Road
Cleveland, Ohio 44135

Dr. R. L. Ashbrook - MS 49-3
NASA Lewis Research Ctr.
21000 Brookpark Road
Cleveland, Ohio 44135

Mr. C. P. Blankenship - MS 105-1
NASA Lewis Research Ctr.
21000 Brookpark Road
Cleveland, Ohio 44135

Dr. H. R. Gray - MS 49-1
NASA Lewis Research Ctr.
21000 Brookpark Road
Cleveland, Ohio 44135

Miss T. D. Gulko - MS 49-3
NASA Lewis Research Ctr.
21000 Brookpark Road
Cleveland, Ohio 44135

Mr. F. H. Harf - MS 49-3   (10)
NASA Lewis Research Ctr.
21000 Brookpark Road
Cleveland, Ohio 44135

Mr. M. Quatinetz - MS 49-3
NASA Lewis Research Ctr.
21000 Brookpark Road
Cleveland, Ohio 44135

Dr. C. W. Andrews - MS 49-3
NASA Lewis Research Ctr.
21000 Brookpark Road
Cleveland, Ohio 44135

Mr. G. M. Ault - MS 3-13
NASA Lewis Research Ctr.
21000 Brookpark Road
Cleveland, Ohio 44135

Mr. J. C. Freche - MS 49-1
NASA Lewis Research Ctr.
21000 Brookpark Road
Cleveland, Ohio 44135

Mr. S. J. Grisaffe - MS 49-3
NASA Lewis Research Ctr.
21000 Brookpark Road
Cleveland, Ohio 44135

Mr. R. W. Hall - MS 49-1
NASA Lewis Research Ctr.
21000 Brookpark Road
Cleveland, Ohio 44135

Dr. H. B. Probst - MS 49-3
NASA Lewis Research Ctr.
21000 Brookpark Road
Cleveland, Ohio 44135

Mr. J. W. Weeton - MS 49-3
NASA Lewis Research Ctr.
21000 Brookpark Road
Cleveland, Ohio 44135

Contracts Section B - MS 500-313
NASA Lewis Research Ctr.
21000 Brookpark Road
Cleveland, Ohio 44135

Patent Counsel - MS 500-113
NASA Lewis Research Ctr.
21000 Brookpark Road
Cleveland, Ohio 44135

Technology Utilization - MS 3-19
NASA Lewis Research Ctr.
21000 Brookpark Road
Cleveland, Ohio 44135

Mr. G. C. Deutsch/RW
NASA Headquarters
Washington, D. C. 20546

Distribution List (continued)

Library
NASA Goddard Space Flight Ctr.
Greenbelt, Maryland 20771

Mr. E. Hasemeyer
NASA S & E-PE-MWM
Marshall Space Flight Ctr.
Huntsville, Alabama 35812

Technical Library/JM6
NASA Johnson Space Ctr.
Houston, Texas 77058

Library
Nasa Flight Research Ctr.
P. O. Box 273
Edwards, California 93523

Library - MS 60-3   (2)
NASA Lewis Research Ctr.
21000 Brookpark Road
Cleveland, Ohio 44135

Report Control Office - MS 5-5
NASA Lewis Research Ctr.
21000 Brookpark Road
Cleveland, Ohio 44135

Lt. Col. H. L. Staubs
AFSC Liaison - MS 501-3
NASA Lewis Research Ctr.
21000 Brookpark Road
Cleveland, Ohio 44135

Mr. J. Maltz/RWM
NASA Headquarters
Washington, D. C. 20546

Library - MS 185
NASA Langley Research Ctr.
Langley Field, Virginia 23365

Library
NASA Marshall Space Flight Ctr.
Huntsville, Alabama 35812

Library - Acquisitions
Jet Propulsion Lab.
4800 Oak Grove Drive
Pasadena, California 91102

Library - Reports - MS 202-3
NASA Ames Research Ctr.
Moffett Field, California 94035

Acquisitions Branch   (10)
NASA Scientific & Tech.
Information Facility
Box 33
College Park, Maryland 20740

Mr. W. J. Schultz
AFML/Headquarters
Wright Patterson AFB, Ohio 45433

Capt. D. W. Zabierek
AFAPL/TBP - Headquarters
Wright Patterson AFB, Ohio 45433

Mr. D. J. Veichnicky AMXMRR
Army Materials and Mechanics Res. Ctr.
Watertown, Massachusetts 02172

Mr. R. J. Schaefer
Code 6350
U. S. Nav. Res. Lab.
Washington, D. C. 20390

Mr. R. E. Trabocco
Physical Metall. Branch
Nav. Air Dev. Ctr.
Warminster, Pennsylvania 18974

Dr. E. G. Zukas
Los Alamos Sci. Lab.
P. O. Box 1663
Los Alamos, NM 87544

Mr. F. Wood
Dept. of Interior
Bureau of Mines
P. O. Box 70
Albany, OR 97321

Mr. J. R. Lane
Materials Adv. Bd.
Nat. Acad. of Sciences
2101 Constitution Ave.
Washington, D. C. 20418

Distribution List (continued)

Dr. D. R. Rossington
Suny College of Ceramics
Alfred University
Alfred, NY 14802

Dr. R. I. Jaffee
Battelle Memorial Inst.
505 King Avenue
Columbus, Ohio 43201

MCIC
Battelle Memorial Inst.
505 King Avenue
Columbus, Ohio 43201

Dr. A. Yue
Department of Metallurgy
University of California
Los Angeles, California 90024

Prof. A. Lawley
Dept. of Metall. Engrg.
Drexel University
Philadelphia, PA 19104

Dr. W. Hertzberg
Dept. Met. & Matl. Sci.
Lehigh University
Bethlehem, PA 18015

Prof. M. C. Flemings
Dept. of Metallurgy
Mass. Inst. of Technology
Cambridge, MA 02139

Prof. G. S. Ansell
Rensselaer Polytechnical Inst.
Troy, NY 12100

Mr. H. E. Boyer
AM. Society for Metals
Metals Park
Novelty, OH 44073

Mr. D. J. Maykuth
Battelle Memorial Inst.
Cobalt Information Ctr.
505 King Avenue
Columbus, OH 43201

Mr. J. M. Dickinson
University of California
Los Alamos Sci. Lab.
P. O. Box 1663
Los Alamos, NM 87544

Mr. T. Z. Kattamis
School of Engineering
University of Connecticut
Storrs, CT 06268

Dr. D. L. Albright
Dept. Met. & Mat. Engrg.
Ill. Inst. of Techn.
Chicago, IL 60616

Dr. W. R. Kraft
Dept. Met. & Matl. Sci.
Lehigh University
Bethlehem, PA 18015

Prof. N. J. Grant
Dept. of Metallurgy
Mass. Inst. of Technology
Cambridge, MA 02139

Dr. B. F. Oliver
Dept. Chem. & Met. Engrg
University of Tennessee
Knoxville, TE 37916

Dr. T. T. Courtney
University of Texas
Matls. Sci. Lab.
Austin, Texas 78712

Mr. B. Goldblatt
Avco Lycoming Div.
550 S. Main Street
Stratford, CT 06497

Dr. J. Denny
Beryllium Corporation
P. O. Box 1462
Reading, PA 19603

Library
Chrysler Corporation
Defense-Space Group
P. O. Box 757
Detroit, MI 48231

Mr. R. E. Engdahl
Deposits & Composites Inc.
1821 Michael Faraday Dr.
Reston, VA 22090

Dr. Y. P. Telang
Materials Development
Ford Motor Company
One Parklane Boulevard
Dearborn, MI 48126

Dr. M.G. Benz
CRD
General Electric Company
P.O. Box 8
Schenectady, N Y 12301

Mr. J.L. Walter
CRD
General Electric Company
P. O. Box 8
Schenectady, NY 12301

Mr. D. M. Goddard
Aerospace Corporation
P. O. Box 95085
Los Angeles, CA 90045

Dr. K. A. Jackson
Bell Telephone Labs.
600 Mountain Avenue
Murray Hill, NJ 07974

Dr. S. T. Wlodek
Stellite Division
Cabot Corporation
1020 W. Park Ave.
Kokomo, IN 46901

Dr. D.L. Sponseller
Climax Molybdenum Company
1600 Huron Parkway
Ann Arbor, Michigan 48106

Mr. C. Zweben
E. I. Dupont & Co.
Textile Fiber Dept.
Wilmington, Delaware 19898

Dr. R. F. Kirby
Garrett Air Research
Dept. 93-393
402 S. 36th Street
Phoenix, AR 85034

Dr. M. F. Henry
CRD
General Electric Co.
P. O. Box 8
Schenectady, NY 12301

Techn. Information Ctr.
AEG
General Electric Co
Cincinnati, Ohio 45215

Dr. C. A. Bruch
AEG/GED
General Electric Co.
Cincinnati, Ohio 45215

Library
Materials Science Lab. W5
Detroit Diesel Allison
General Motors
Indianapolis, IN 46206

Mr. W. H. Freeman
Superalloy Group
Howmet Corporation
Whitehall, MI 49461

Mr. R. C. Gibson
International Nickel Co.
Merica Research Lab.
Sterling Forest
Suffern, NY 10901

Dr. L. Kaufman
Manlabs, Inc.
21 Erie Street
Cambridge, MA 02139

Mr. R. A. Alliegro
Refractories Division
Norton Company
Worcester, MA 01606

Distribution List (continued)

Dr. W. Sutton
Special Metals Corporation
New Hartford, NY 13413

Library
Materials Technology
TRW Equipment Group
23555 Euclid Avenue
Cleveland, OH 44117

Dr. M. Herman
Detroit Diesel Allison DV
P. O. Box 894
Indianapolis, IN 46206

Dr. E. E. Reynolds
Technical Ctr.
General Motors Corp.
Warren, MI 48090

Dr. R. F. Decker
International Nickel Co.
One New York Plaza
New York, NY 10004

Technical Information Ctr.
Matls. & Science Lab.
Lockheed Research Labs.
3251 Hanover Street
Palo Alto, Cal. 94304

Mr. C. E. Nelson
National Beryllia Corp.
First and Haskell Ave.
Haskell, NJ 07420

Dr. G. Garmong
Rockwell International
Science Ctr.
Thousand Oaks, California 91360

Dr. T. Piwonka
Materials Technology
TRW Equipment Group
23555 Euclid Avenue
Cleveland, OH. 44177

Dr. P. S. Kotval
Union Carbide - Research Institute
Tarrytown, NY 10591

Dr. F. D. Lemkey
United Aircraft Corp.
Research Laboratories
East Hartford, CT 06108

Dr. R. H. Barkalow
Pratt & Whitney Aircraft
United Aircraft Corp.
400 Main Street
East Hartford, CT 06108

Dr. M. L. Gell
Pratt & Whitney Aircraft
United Aircraft Corp.
400 Main Street
East Hartford, CT 06108

Dr. K. D. Scheffler
Pratt & Whitney Aircraft
United Aircraft
400 Main Street
East Hartford, CT 06108

Dr. E. R. Thompson
United Aircraft Corp.
Research Laboratories
East Hartford, CT 06108

Dr. J. S. Erickson
Pratt & Whitney Aircraft
United Aircraft Corp.
400 Main Street
East Hartford, CT 06108

Dr. G. R. Leverant
Pratt & Whitney Aircraft
United Aircraft Corp.
400 Main Street
East Hartford, CT 06108

Dr. R. H. Hopkins
Westinghouse Research Lab.
Beula Road
Pittsburgh, Pennsylvania 15235